HAL open science

Ca-Sr isotope and chemical evidence for distinct sources of carbonatite and silicate mantle metasomatism

Hongli Zhu, Dmitri Ionov, Long Du, Zhaofeng Zhang, Weidong Sun

To cite this version:

Hongli Zhu, Dmitri Ionov, Long Du, Zhaofeng Zhang, Weidong Sun. Ca-Sr isotope and chemical evidence for distinct sources of carbonatite and silicate mantle metasomatism. Geochimica et Cosmochimica Acta, 2021, 312, pp.158-179. 10.1016/j.gca.2021.08.004 . hal-03402764

HAL Id: hal-03402764

https://hal.science/hal-03402764v1

Submitted on 16 Oct 2023

HAL is a multi-disciplinary open access archive for the deposit and dissemination of scientific research documents, whether they are published or not. The documents may come from teaching and research institutions in France or abroad, or from public or private research centers.

L'archive ouverte pluridisciplinaire **HAL**, est destinée au dépôt et à la diffusion de documents scientifiques de niveau recherche, publiés ou non, émanant des établissements d'enseignement et de recherche français ou étrangers, des laboratoires publics ou privés.

Distributed under a Creative Commons Attribution - NonCommercial 4.0 International License

Version of Record: https://www.sciencedirect.com/science/article/pii/S0016703721004701
Manuscript_8378c667c77edc9698df89544b0ef3e4

Ca-Sr isotope and chemical evidence for distinct sources of carbonatite and silicate mantle metasomatism

Hongli Zhu[a,b,c], Dmitri A. Ionov*[d,e], Long Du[f], Zhaofeng Zhang[e,g], Weidong Sun[a,b,c]

[a] *Center of Deep Sea Research, Institute of Oceanography, Chinese Academy of Sciences, Qingdao 266071, China*

[b] *Laboratory for Marine Mineral Resources, Pilot National Laboratory for Marine Science and Technology (Qingdao), Qingdao 266237, China*

[c] *Center for Ocean Mega-Science, Chinese Academy of Sciences, Qingdao 266071, China*

[d] *Géosciences Montpellier, University of Montpellier, CNRS, Montpellier 34095, France*

[e] *State Key Laboratory of Isotope Geochemistry, Guangzhou Institute of Geochemistry, Chinese Academy of Sciences, Guangzhou 510640, China*

[f] *College of Earth Science and Engineering, Shandong University of Science and Technology, Qingdao 266590, China*

[g] *International Center for Planetary Science, College of Earth Sciences, Chengdu University of Technology, Chengdu 610059, China*

8898 words in the main text, 4 tables, 9 figures, Supplementary material; 98 references

© 2021 published by Elsevier. This manuscript is made available under the CC BY NC user license
https://creativecommons.org/licenses/by-nc/4.0/

Abstract *(404 words)*

Enrichments in light REE without concomitant enrichments in high-field-strength elements in mantle peridotites are usually attributed to inputs from carbonate-rich melts and referred to as 'carbonatite' metasomatism as opposed to interaction with evolved silicate melts. Alternatively, both enrichment types are ascribed to percolating volatile-bearing mafic liquids whose chemical signatures evolve from 'silicate' to 'carbonatite'. Here we compare these models for peridotites in which these enrichment types are combined, as may be common in the mantle. We report new Ca-Sr-Nd isotope and chemical data for lherzolite and harzburgite xenoliths from Spitsbergen that were metasomatized, first, by silicate, then by carbonate-rich melts that formed carbonate-bearing pockets replacing earlier minerals. Seven crushed samples were treated with acetic acid that dissolved carbonates formed in the latest event, but not silicates. The leachates (acid-removed carbonates making up 0.6–1.4% of total sample mass) contain much more Sr than the residues after leaching (277–2923 vs. 16–60 ppm), have a greater overall $^{87}Sr/^{86}Sr$ range (0.7049–0.7141 vs. 0.7036–0.7055) and higher $^{87}Sr/^{86}Sr$ in each sample than the residues. The leachates have lower $\delta^{44/40}Ca$ range (0.17–0.68‰) than the residues (0.78–1.00‰), as well as lower $\delta^{44/40}Ca$ than the residues in all samples but one. By and large, the carbonates are out of Ca-Sr isotope equilibrium with the host peridotites implying that the older silicate and younger carbonatite metasomatism were produced by different parental melts, thus supporting the existence of distinctive carbonate-rich metasomatic media in the lithospheric mantle, possibly including recycled materials.

The $\delta^{44/40}Ca$ in the leachates (i.e. carbonates, 0.17–0.68‰) are well below bulk silicate Earth (BSE) estimates (0.94 ± 0.05‰) and $\delta^{44/40}Ca$ in non-metasomatized melt-depleted mantle. Yet, $\delta^{44/40}Ca$ in the non-leached whole rock (WR) carbonate-bearing samples (0.75–0.95‰) fall within, or are only slightly lower than, the BSE range. The $^{87}Sr/^{86}Sr$ range in these WR samples (0.7030–0.7112) includes very high values for peridotites with large aggregates of dolomite and Mg-calcite. It

appears that both carbonatite and silicate metasomatism may produce $\delta^{44/40}$Ca values lower than the BSE such that Ca-isotope data cannot robustly tell apart these two enrichment types, yet carbonatite metasomatism may yield the lowest $\delta^{44/40}$Ca. Carbonates, even at small mass fractions, are significant hosts of Sr in the WR Spitsbergen peridotites (8–51 wt.% of Sr mass) because of very high Sr concentrations, but add little to WR Ca balance (3–12 wt.%). As a result, high Sr content and ^{87}Sr/^{86}Sr ratios may be indices (though not definitive proofs) of carbonatite metasomatism in mantle rocks.

Key words: carbonatite metasomatism; silicate metasomatism; Ca isotopes; Sr isotopes; mantle xenolith; peridotite; Spitsbergen

1. INTRODUCTION

Studies of chemical and mineralogical composition of mantle rocks suggested that they were affected by two types of metasomatism, 'silicate' and 'carbonatite', the latter characterized by strong enrichments in light rare earth elements (LREE) at low high-field-strength elements (HFSE) (Ionov et al., 1993; Rudnick et al., 1993; Yaxley et al., 1991). These results implied an important, widespread role for carbonatite melts as agents of mantle metasomatism, despite the rarity of these melts at the Earth's surface (Hauri et al., 1993). However, other studies on mantle xenoliths and peridotite massifs inferred that enrichment patterns similar to those attributed to carbonate-rich melts could be produced by reactive percolation of volatile-bearing silicate melts. Numerical modeling of this process (Navon and Stolper, 1987) obtained a range of chemical patterns from a single parental liquid at different distances from its source as a result of chromatographic fractionation (due to different element compatibility), with 'carbonatite' signatures at the percolation front (e.g. Bodinier et al., 1990; Ionov et al., 2002a).

The existence of distinct, carbonatite and silicate, agents of mantle metasomatism can be ascertained using isotope compositions, which may differ in samples affected by media generated from different sources, but are similar in samples reworked by derivatives of a single initial agent. Here we present new Ca-Sr-Nd isotope and trace element data for a suite of mantle peridotites from the island of Spitsbergen that contain carbonate-bearing pockets of mantle origin replacing earlier minerals (Ionov et al., 1993; Ionov et al., 1996). Calcium and strontium are typical chemical components of carbonatites. The main objective of this study is to distinguish the Ca-Sr isotope inputs of the carbonates in the rocks using leaching with acetic acid that dissolves only carbonates. The data are used to evaluate directly the effects of carbonate-rich liquids on mantle metasomatism as well as to establish whether different types and stages of metasomatism were produced by distinct types and

sources of media.

Calcium is a major lithophile element in the Earth's mantle and crust (e.g. Hofmann, 1988). It has six naturally occurring stable isotopes (^{40}Ca, ^{42}Ca, ^{43}Ca, ^{44}Ca, ^{46}Ca and ^{48}Ca) with ~10% mass difference ($\Delta m/m$) between ^{40}Ca and ^{44}Ca (DePaolo, 2004). Calcium isotopic compositions are usually expressed as delta notation, e.g. $\delta^{44/40}$Ca relative to NIST SRM 915a: $[(^{44}Ca/^{40}Ca)_{sample}/(^{44}Ca/^{40}Ca)_{NIST\text{-}SRM\text{-}915a} - 1] \times 1000$.

The application of Ca stable isotopic composition in geosciences has rapidly developed in the last two decades because Ca isotopes show important fractionation at low temperatures near the Earth's surface, and are considered important indices of a wide range of biological and chemical processes in sedimentology, environmental geochemistry, weathering etc. (e.g. Blättler and Higgins, 2017; DePaolo, 2004; Fantle and Tipper, 2014; Farkaš et al., 2007; Skulan et al., 1997). Ca isotopes may also give new insights into global reservoirs and high-temperature processes in the Earth's interior and extraterrestrial samples (see Antonelli and Simon (2020) for a review).

Recent studies revealed significant Ca isotope variations in mantle-derived mafic igneous rocks (Huang et al., 2011; Liu et al., 2017a; Zhu et al., 2020; Zhu et al., 2018b) and carbonatites (Amsellem et al., 2020; Banerjee and Chakrabarti, 2019; Banerjee et al., 2021; Sun et al., 2021). Ca isotope variations were reported also for the lithospheric mantle and ascribed to additions of recycled crustal materials (Chen et al., 2018; Huang et al., 2011; Liu et al., 2017a; Zhu et al., 2020; Zhu et al., 2018b) and/or equilibrium and disequilibrium isotope fractionation at high temperatures during: (a) melt extraction (Chen et al., 2019; Kang et al., 2017), (b) reaction with silicate and carbonate-rich melts or fluids (Ionov et al., 2019; Kang et al., 2017; Kang et al., 2019; Kang et al., 2016; Zhao et al., 2017). This opens up new prospects in mantle studies, but also creates new challenges, in particular how to distinguish Ca isotope variations in mantle rocks produced by intra-mantle fractionation from those caused by mixing with recycled crustal materials.

An important notion in mantle studies is that of the Bulk Silicate Earth (BSE), sometimes called "primitive mantle" (PM), defined as silicate portion of the Earth as it existed after separation of the core but before it was differentiated to crust and heterogeneous mantle (Hofmann, 1997). Present-day mantle reservoirs were formed by melt extraction from the BSE (Workman and Hart, 2005), metasomatism and recycling of surface materials. The BSE composition may be evaluated using fertile mantle peridotites that experienced no melt extraction or metasomatism (Palme & O'Neill, 2003; McDonough & Sun, 1995). So far, the only robust $\delta^{44/40}$Ca estimate for the BSE (0.94 ± 0.05‰, 2sd) has been given by Kang et al. (2017) based on 14 xenoliths of non-metasomatized fertile lherzolites with Al_2O_3 (3.7–4.7 wt.%) and CaO (3.2–4.0 wt.%) overlapping the PM estimates (~4.5 and 3.6%, respectively).

Kang et al. (2017) obtained a higher than BSE average $\delta^{44/40}$Ca (1.06 ± 0.06‰, 2sd) for strongly melt-depleted (1.3–1.7 wt.% Al_2O_3), non-metasomatised (LREE-depleted) peridotites and suggested that high degrees of melt extraction produce slightly higher (by ~0.12‰) $\delta^{44/40}$Ca in residues. A similar $\delta^{44/40}$Ca range (and $\delta^{44/40}$Ca evolution trend during melting) was found by Chen et al. (2019) in melt-depleted lherzolites from Alpine massifs. Kang et al. (2017) also reported usually lower $\delta^{44/40}$Ca (0.25–0.96‰) in metasomatized (LREE-enriched) peridotites, in particular for low-CaO (≤1 wt.%) rocks with Ca budget dominated by metasomatic inputs.

Strontium, like Ca, is an alkali earth element, but its BSE abundance is three orders of magnitude lower (20 vs. 25400 μg/g). Strontium is highly incompatible during peridotite melting because cation Sr^{2+} is much larger than Ca^{2+} such that Sr partition coefficients between clinopyroxene (major Sr host in common lherzolites) and mafic melts are well below unity (https://earthref.org/KDD/e:38/). Using the Rb-Sr radiogenic isotope system for dating mantle materials is problematic due to high mobility of these elements (e.g. Pearson et al., 2014), but the $^{87}Sr/^{86}Sr$ ratios may indicate the sources of mantle-derived rocks and magmas (Hofmann, 2003), as well as recycling of crustal materials (e.g. Guo et al., 2020; Xu, 2002). The $^{87}Sr/^{86}Sr$ ratios in

mantle rocks are affected both by their age and the evolution of the Rb/Sr ratio that may be hard to disentangle to identify sources of metasomatism. By comparison, Ca isotope compositions do not evolve with time, but may reveal mantle sources, mixing or, alternatively, mass-dependent fractionation during mantle processes. Overall, the evidence from Sr and Ca isotopes may be complementary.

Previous studies found carbonates usually associated with (Na,Al)-rich silicate glass in some Spitsbergen xenoliths (Ionov et al., 1993; Ionov et al., 1996). The carbonates do not represent quenched carbonatite liquids but are crystal cumulates from carbonate-rich silicate melts reacting with host peridotites (Ionov and Harmer, 2002). Trace element patterns estimated for such liquids (Ionov, 1998) are consistent with many features of 'carbonatite' metasomatism (enrichments in LREE, Sr, Ba and negative HFSE anomalies). However, similar element patterns were found also in peridotites that contain no carbonates and attributed to reactive percolation and extreme fractionation of volatile-bearing silicate melts (Ionov et al., 2002a).

Overall, it remains uncertain whether the carbonates in mantle xenoliths from Spitsbergen and other worldwide localities (e.g. Dautria et al., 1992; Ionov et al., 2018; Laurora et al., 2001) originate from particular carbonate-rich liquids or are late-stage derivatives of evolving volatile-bearing silicate melts. In a more general sense, the ambiguity concerns the origin of chemical signatures usually seen as evidence for 'carbonatite' mantle metasomatism (e.g. Rivalenti et al., 2004; Tappe et al., 2017).

This uncertainty is addressed here using Ca-Sr isotope and chemical data on carbonate-bearing Spitsbergen xenoliths, notably by treating WR samples with acetic acid that dissolves only carbonates. Analyses of the leachates, residues and bulk-rocks discern metasomatic inputs of late-stage carbonates (extracted by leaching) from those of earlier events (hosted by residues). We show that trace element patterns and Ca-Sr isotope compositions of the leachates, hence carbonates, are distinct from those in the silicate minerals of the host peridotites. We infer that the carbonate pockets were

formed from specific carbonate-rich liquids responsible for 'carbonatite' metasomatism. We further discuss the application of Ca-Sr isotope data to gain insights into the sources and mechanisms of metasomatism in the mantle.

2. GEOLOGICAL SETTING AND SAMPLES

Spitsbergen is the largest island of the Svalbard archipelago, the northwestern (NW) edge of the Eurasian continent. It was connected to Greenland until the opening of the North Atlantic Ocean, and is located now ~200 km east of the mid-ocean ridge (e.g. Vagnes and Amundsen, 1993), between the North Atlantic and the Arctic Oceans at similar distances from Norway, Greenland and the North Pole.

Mantle xenoliths reported here were collected in alkali basaltic rocks at three Quaternary eruption centers in NW Spitsbergen: Sverre, Halvdan and Sigurd (e.g. Griffin et al., 2012). Most of the xenoliths are coarse to medium-grained spinel lherzolites containing 5–12% clinopyroxene (Ionov et al., 2002a; Ionov et al., 1996); samples 26A and 318 are harzburgites (Streckeisen, 1976). The samples from Sverre are mainly 'anhydrous' lherzolites, while the Halvdan peridotites usually contain amphibole with modal abundances ranging from rare grains in sample 4-90-9 to 5–8% in samples 318 and 315-6. Samples 21-6 and 43-86 have accessory apatite (S-Fig. 1a in Electronic Appendix 2 (EA2)). The peridotites equilibrated at 840–990°C based on two-pyroxene thermometry (Ionov et al., 2002a). Sample 4A-90-1 from Sigurd is a coarse-grained clinopyroxene-amphibole vein.

The xenoliths contain carbonates as mosaic aggregates of dolomite and Mg-calcite with smooth curvilinear boundaries made up of interlocking grains 20–50 μm in size (Ionov, 1998; Ionov et al., 1993; Ionov et al., 1996). They mainly occur in irregularly distributed pockets that typically make up ≤ 2–3% of the rock and are 0.2–2 mm in size. The pockets also contain small (<100 μm) euhedral grains of clinopyroxene and olivine, Fe-Ni sulfides and (Na,Al)-rich silicate glass with micro-phenocrysts of Cr-rich spinel (S-Fig. 1d-h, EA2). The pockets replace minerals of host peridotite,

usually orthopyroxene, amphibole and spinel, that have embayed, resorbed outlines and spongy reaction zones. Less commonly the carbonates occur as mosaic aggregates in veins and at grain junctions of silicates (S-Fig. 1b-c, EA2).

Such assemblages closely resemble experimental and natural evidence for mantle-derived carbonatite metasomatism (e.g. Green and Wallace, 1988). Studies of melt and fluid inclusions in other carbonate-bearing, metasomatized mantle xenoliths suggest that carbonate segregations formed from initially homogeneous silicate-carbonate melts that separate into carbonatite and silicate components when they intrude and react with host peridotites (Frezzotti et al., 2002; Laurora et al., 2001).

The carbonate globules are larger and more abundant in four out of seven xenoliths selected for leaching (samples 43-86, 4-36-90, 4-90-9 and 21-6). Some carbonate aggregates are altered at rims to fine grained and turbid materials consisting of composite microcrystalline (usually magnesite-ankerite) spherules immersed in amorphous Mg-rich silicate material with low totals (S-Fig. 1g). They are common in samples SB-4 and 28B (Ionov et al., 1993), but their proportions relative to primary carbonates are negligible in large pockets (samples 43-86, 4-36-90, 4-90-9 and 21-6).

Textural evidence suggests that the Mg-Fe-rich carbonates formed by alteration of primary dolomite and Mg-calcite in contact with silicates during the eruption, likely due to heating and pressure drop. However, no evidence exists for the formation of additional carbonates in low-temperature processes. Na-rich silicate glass in contact with carbonates is not altered and contains fresh sulfide globules (Ionov et al., 1996). The silicate glass in the xenoliths is very different from the glass in the host basaltic rocks in terms of color, phenocryst assemblage and chemical composition, which rules out links with host magma infiltration (Ionov et al., 1993).

Previous chemical and isotope studies of Spitsbergen xenoliths, including those that contain no carbonates, found combined effects of three discrete evolution stages. (1) The protoliths for the lithospheric mantle were formed by melt extraction from

fertile mantle with melting degrees ranging from <10% for some lherzolites to 25% for the harzburgites in the Paleoproterozoic that depleted the rocks in incompatible elements (Choi et al., 2010; Ionov et al., 2002a). (2) The melting residues were then metasomatized by silicate liquids to form amphibole and apatite as well as enrich the residues in incompatible elements (Ionov et al., 2002a), radiogenic Sr isotopes (0.7025–0.7036) and non-radiogenic Nd isotopes (0.5123–0.5136) (Ionov et al., 2002b). (3) Ingress of carbonate-rich media formed discordant carbonate-bearing pockets shortly before the eruption of host magma (Ionov, 1998).

Ionov et al. (2002a) outlined two types of trace element patterns in WR samples and coarse silicate minerals of Spitsbergen xenoliths (Type-1 and Type-2) that combine features attributed to silicate or carbonatite metasomatism, e.g. negative Ti-Zr-Hf anomalies in Type-2 rocks and strongly fractionated LREE with high La/Ce (and H_2O/Ce, Tang et al. (2020)) in Type-1 bulk-rocks and clinopyroxene. Ionov et al. (2002a) argued that the remarkable enrichments in the least compatible elements, along with fractionation of elements with similar compatibility, in Type 1 samples may not be due to mixing of melting residues with common enriched mafic melts but to extreme fractionation near melt percolation front. They used numerical modelling of reactive porous flow of volatile-bearing silicate liquids in depleted peridotites to explain their trace element patterns and Sr-Nd isotope ratios (Ionov et al., 2002a; Ionov et al., 2002b). Those studies, however, did not address specifically xenoliths containing late-stage carbonates and pockets of fine-grained minerals and silicate glass. They did not establish the provenance of carbonate-rich media responsible for carbonate formation, particularly whether they are related to late-stage derivatives of silicate metasomatism in the Spitsbergen mantle.

3. SAMPLE TREATMENT AND ANALYTICAL METHODS

The xenoliths analyzed in this study are listed in Table 1, along with a summary of

information on available data from this and previous studies.

3.1 Leaching experiments

Acid-leaching experiments were done on seven carbonate-bearing peridotites to obtain separately the compositions of carbonates and silicates (as well as spinel and apatite) in each sample. Our approach is different from that employed by Ionov et al. (1993) who leached two of these samples (Table 1) with 10% HNO_3 for about 20 minutes in an ultrasonic bath, which did not only dissolve carbonates but may have also affected other phases, e.g. silicate glass. In this study, the samples were treated with dilute acetic acid (HAc), which dissolves carbonates while leaving silicate and oxide phases intact. Specifically, aliquots of 4–10 g of rock were crushed by hand to ≤1 mm in an agate mortar. These samples were transferred to centrifuge tubes and weighed. About 15 ml of 10% HAc were added to the centrifuge tubes, which usually produced gas bubbles; the tubes were shaken for about 30 min. The samples were centrifuged and the leachates (solutions with dissolved carbonates) extracted by pipette; the leaching residues were washed twice with MQ water, which was added to the initial leachates.

To convert the acetate salts in the leachates to nitrates and remove remaining HAc, the leachate solutions were dried and treated with concentrated HNO_3 several times on a hot plate at 150°C until clear solutions were obtained, then transferred to Teflon beakers. The solutions were dried, and dissolved in 2M HNO_3 for major and trace element and Sr-Nd-Ca isotopic analysis.

After the leachate extraction, the residues were dried overnight at 105°C and weighed to calculate the mass loss on leaching, and the relative mass of the carbonate and acid-resistant components in each sample. Finally, the leaching residues were ground to 200 mesh powder for analyses.

3.2 Major and trace elements

Major and trace element concentrations were obtained in this study for leachates

and residues from seven xenoliths, as well as for six WR samples (non-leached). Another six WR samples were analyzed for major elements only. We also use WR major and trace element data on 17 Spitsbergen xenoliths reported earlier (Ionov et al., 2002a; Ionov et al., 1993; Ionov et al., 1996).

The major and trace element analyses were done at the State Key Laboratory of Isotope Geochemistry (SKLIG), Guangzhou Institute of Geochemistry (GIG), Chinese Academy of Sciences (CAS). About 80 mg of residue or WR powder was fully digested in Teflon beakers with HF-HNO_3 mixtures placed in steel-jacketed PARR bombs following procedures reported in Wang et al. (2018). These solutions were used for both major and trace element, and Ca-Sr-Nd isotopic analyses.

Major elements (except Si) were analyzed by inductively coupled plasma atomic emission spectrometry (ICP-AES); Chinese reference samples GSR-1, GSR-2, GSR-3, SARM-4 and SY-4 were used for external calibration. Repeated analyses of USGS reference materials indicate external reproducibility better than 10%. Trace elements were determined by ICP mass spectrometry (ICP-MS) following procedures reported in Du et al. (2018) with reproducibility better than 5%.

3.3 Sr-Nd isotopes

Chemical separation and isotope analyses of Sr and Nd were done at the SKLIG-GIG-CAS. Aliquots of sample solution containing ~800 ng of Sr were transferred to a Teflon beaker, dried, and dissolved in 0.25 ml of 3 M HNO_3. To separate Sr from sample matrix, the sample solution was loaded onto a column packed with 0.25 ml of Sr Spec resin (Zhu et al., 2018b). After elution by 6.5 ml of 3 M HNO_3, Sr was collected in 3 ml of 0.05 M HNO_3. Strontium isotopes were measured on a Nu Plasma 1700 multi-collector (MC) ICP-MS instrument. The $^{87}Sr/^{86}Sr$ ratios were corrected for instrumental mass fractionation by normalizing to $^{88}Sr/^{86}Sr = 8.375209$. The $^{87}Sr/^{86}Sr$ values obtained for reference materials NBS-987 (0.710254 ± 0.000014; 2sd, n = 12) and BHVO-2 (0.703503 ± 0.000009; n = 1, internal precision) are consistent with

literature data (Table 2) (Charlier et al., 2006; Meng et al., 2019; Thirlwall, 1991; Weis et al., 2006).

More than half of the leachates, residues and WR samples are too low in Nd for precise Nd isotope analyses. Neodymium was purified using a two-column procedure reported in Du et al. (2019) and Ma et al. (2013). The first column filled with 1 g of AG50W-X12 (200–400 mesh) resin was eluted with 2.5 M HCl to extract the REE. Neodymium was separated from other REE on the second column filled with 1 g of Ln Spec (50–100 mesh) resin and eluted with 0.25 M HCl. The isotopic ratios were measured on a Nu Plasma 1700 MC-ICP-MS. The $^{143}Nd/^{144}Nd$ values for reference materials JNdi (0.512111 ± 0.000013; 2sd, n = 13) and W-2 (0.512512 ± 0.000008; n = 1, internal precision) agree within error with literature data (Li et al., 2012; Luo et al., 2020; Tanaka et al., 2000) as shown in Table 2.

3.4 Calcium isotopes

Chemical purification and analyses of Ca isotope compositions were done at the SKLIG-GIG-CAS following procedures in Zhu et al. (2018a), Zhu et al. (2016) and Liu et al. (2017b). An aliquot of sample solution containing 30–50 μg of Ca was mixed with a ^{42}Ca-^{43}Ca double-spike solution containing 8 μg Ca, dried, re-dissolved in 0.1 ml of 1.6 M HCl, loaded onto a column filled with 1 ml of AG MP-50 (100–200 mesh) and eluted with 1.6 M HCl. Most of the matrix was eluted with 17 ml of 1.6 M HCl, then Ca was collected in 27 ml of 1.6 M HCl. Samples low in CaO (< 3 wt.%) were passed through the column twice. The Ca recovery was >99%. Column chemistry was run in batches of 20 samples; at least one reference material and blank were processed as unknowns with each batch. Total procedure blanks were 15–70 ng, which is negligible compared to 30–50 μg of Ca loaded onto the column.

Calcium isotopic compositions were measured on a 'Thermo Triton' thermal ionization mass-spectrometer (TIMS). About 1 μl 10% HNO_3 containing 5 μg Ca was loaded onto the center of out-degassed single Ta (99.995%) filament. A droplet of 1 μl

activator (10% H_3PO_4) was loaded to cover the sample spot. A single sequence of cup configuration was adopted with ^{40}Ca, ^{41}K, ^{42}Ca, ^{43}Ca and ^{44}Ca collected in L2, C, H1, H2 and H3 Faraday cups, respectively. ^{41}K was measured to evaluate isobaric interference of ^{40}K on ^{40}Ca, and an online correction was done using $^{40}K/^{41}K = 1.7384 \times 10^{-3}$ Heuser et al. (2002). Instrumental fractionation was corrected using the ^{42}Ca-^{43}Ca double spike method similar to that of Heuser et al. (2002) with the exponential fractionation law. The Ca isotope data are reported as $\delta^{44/40}Ca$ relative to NIST SRM 915a. NIST SRM 915a and IAPSO seawater reference materials were routinely measured to monitor instrumental stability. Two standard deviation (2sd) of average $\delta^{44/40}Ca$ for NIST SRM 915a analyzed in the course of this study was 0.12‰ (n = 34). Three to seven aliquots of each sample solution were loaded on different filaments and measured separately; the reproducibility of $\delta^{44/40}Ca$ in the duplicate analyses of each sample is ± 0.08‰ (2SE, see footnote of Table 3).

The $\delta^{44/40}Ca$ values for NIST SRM 915a, IAPSO seawater and four USGS reference materials (DTS-1, DTS-2, PCC-1 and BHVO-2) measured in the same session, and literature data are listed in Table 2. Average $\delta^{44/40}Ca$ values obtained for NIST SRM 915a and IAPSO seawater are -0.02 ± 0.12‰ (2sd, n = 21) and 1.82 ± 0.10‰ (2sd, n = 10), respectively; those of DTS-1, DTS-2, PCC-1 and BHVO-2 are 1.61 ± 0.09‰ (2sd, n = 3), 1.10 ± 0.11‰ (2sd, n = 3), 1.10 ± 0.08‰ (2sd, n = 3) and 0.84 ± 0.09‰ (2sd, n = 5), respectively. These results are consistent with data reported in the literature (Amini et al., 2009; Farkaš et al., 2007; Feng et al., 2017; He et al., 2017; Huang et al., 2010; Valdes et al., 2014). Two WR samples were replicated by digestion of a separate powder batch; one leachate was duplicated by processing in column chemistry (Table 3). Duplicate $\delta^{44/40}Ca$ values for all the three samples are within analytical uncertainty (Table 3).

4. RESULTS

Major and trace element compositions of leachates, residues and WR xenoliths in this study are listed in S-Tables 1 and 2 of Electronic Appendix 1 (EA1) along with relevant literature data (Ionov et al., 2002a; Ionov et al., 1993; Ionov et al., 1996). The Ca-Sr-Nd isotope compositions obtained in this study are given in Tables 3 and 4. Acid leaching was used here to separate the metasomatic inputs of late-stage carbonates (extracted by leaching) from those of earlier melt extraction and silicate metasomatism hosted by residues (Ionov et al., 2002a; Ionov et al., 2002b).

4.1 Chemical compositions

The totals of the leachate analyses are low (46–63 wt.%) due to release of CO_2 from carbonates (44–48 wt.% in pure calcite and dolomite). The main components of the leachates are CaO, MgO and FeO. Their proportions range broadly and outline two end-members. Leachates from xenoliths 4-36-90, 4-90-9 and 21-6 contain 21–33 wt.% CaO, 12–20% MgO and 2.2–3.4% FeO, with higher CaO than for MgO in each case. The leachate 43-86 has less CaO (20 wt.%) than MgO (27 wt.%). Leachates from the other three xenoliths (63-90-18, SB-4 and 28B) are low in CaO (9–15 wt.%) and have two to four times more MgO (34–37 wt.%) and 11–14 wt.% FeO.

Selected chemical data on WR samples and residues after leaching are plotted in Fig. 1 vs. Al_2O_3 together with data on fertile to melt-depleted peridotites from Tariat in Mongolia (Ionov and Hofmann, 2007). Leached residues of the Spitsbergen xenoliths generally have lower Sr, CaO and Ca/Al ratios than the WR samples, in line with the removal of Ca-Sr-rich carbonates. However, all but one residues have higher CaO and Ca/Al than melt-depleted mantle (Fig. 1a), but show no Sr enrichments (Fig. 1c). The leachates contain much more Sr (277–2923 ppm) than the residues (16–60 ppm) (S-Table 2). The Ca-rich leachates from three xenoliths have much more Sr (2337–2923 ppm) than the other four (277–455 ppm). Mass fractions of the leachates range from 0.6 to 1.4% of the bulk rocks (Table 3), in line with the mass fractions of carbonates (~1%) estimated by Ionov et al. (1993). Altogether, the data suggest that

leaching entirely removed the metasomatic carbonates from the WR samples.

Ionov et al. (2002a) outlined two types of PM-normalized (McDonough and Sun, 1995) trace element patterns in WR Spitsbergen xenoliths. Our data (Fig. 2) show that the patterns for Type-1 peridotites are nearly flat for heavy to medium REE (HREE-MREE) with steep La-Ce-Pr inflections, while Type-2 peridotites show a continuous decrease in normalized REE from Ce to Ho (Fig. 2a and c). As a result, Type-1 peridotites have lower MREE/HREE and higher La/Ce ratios than Type-2 peridotites.

Both types have strong negative Nb and Ta anomalies; all WR Type-1 peridotites and the majority of Type-2 peridotites show positive Sr anomalies (Fig. 2b and d). Because of the high MREE levels, Type-2 peridotites seem to have larger negative Zr, Hf and Ti anomalies (Fig. 2d) even though the abundances of these elements are similar to those in Type-1 peridotites. Three samples cannot be grouped with either Type-1 or Type-2 (Fig. 2e, f). Among the leached samples with mainly Ca-rich carbonates, one (4-36-90) is of Type 1 while the other three are of Type 2.

Trace element abundances and patterns for leaching residues and WR samples in this study (Fig. 3) are similar to those for two samples reported by Ionov et al. (1993). The concentrations of incompatible trace elements in the leachates in this study, calculated relative to the mass of leached materials, are lower than those reported by Ionov et al. (1993) when plotted relative to 1% of mass of WR samples. The leaching with 10% HNO_3 in the previous work may have dissolved more material than the leaching with 10% HAc in this study. The leachates contain more REE and large ion lithophile elements (Cs, Rb, Ba), but less HFSE than leaching residues and bulk rocks (Figs. 3–5). Besides, the leachates and the residues display the same Type-1 and Type-2 REE patterns, but the leachates have the deepest HFSE anomalies (Fig. 5).

4.2 Sr-Nd isotope compositions

The WR Spitsbergen xenoliths in this study show a broad overall $^{87}Sr/^{86}Sr$ range

(0.7030–0.7112; Fig. 6a), with $^{87}Sr/^{86}Sr$ values in four samples (0.708–0.711) much higher than in the other eleven samples (~0.703–0.704). Three out of seven leached samples have the most radiogenic Sr, the highest Sr (and Ca) concentrations in the leachates and also contain large, least altered carbonate pockets. In general, the WR $^{87}Sr/^{86}Sr$ ratios in this study are higher than those for pure clinopyroxene and amphibole separates from the same samples reported by Ionov et al. (2002b) (Fig. 7b and S-Fig. 2a). Our WR data show no apparent differences in $^{87}Sr/^{86}Sr$ between Type-1 and Type-2 peridotites, unlike data of Ionov et al. (2002b) who found that clinopyroxene has less radiogenic $^{87}Sr/^{86}Sr$ in Type-1 than in Type-2 peridotites. Few samples were measured for Nd isotopes here because of low Nd abundances. The WR $^{143}Nd/^{144}Nd$ range in this study (0.51218–0.51295; Fig. 6b) is narrower than for pure amphibole and clinopyroxene reported by Ionov et al. (2002b) (S-Fig. 2b).

The leachates, leaching residues and WR samples for each xenolith have distinct Sr isotopic compositions (Fig. 7b). The $^{87}Sr/^{86}Sr$ in the leachates (0.7049–0.7141) have a wider range and are generally higher than in the residues (0.7036–0.7055). For a given xenolith, the WR sample has $^{87}Sr/^{86}Sr$ ratios in-between those for leachates and residues.

Unlike for Sr isotope ratios, the leachates, residues and WR samples have similar Nd isotopic compositions (Fig. 7c), consistent with low Nd in the carbonates (Ionov, 1998). The leachates contain only 1–7 wt.% of the total Nd in the bulk rocks (Table 3). The Sr and Nd isotope ratios in the leachates and the residues are positively correlated (Fig. 8b, c).

4.3 Calcium isotopic compositions

The $\delta^{44/40}Ca$ values in the WR Spitsbergen peridotites range from 0.73 to 0.89‰ (Fig. 6a), i.e. are slightly lower than the BSE estimate (0.94 ± 0.05‰; Kang et al. (2017)). There is no obvious difference between Type-1 and Type-2 xenoliths with $\delta^{44/40}Ca$ ranges of 0.78–0.89‰ and 0.73–0.87‰, respectively and between two

groups of leached samples based on Ca-Mg-Fe proportions in the leachates. The $\delta^{44/40}$Ca range for leaching residues (0.78–1.00‰) extends to slightly higher values than for the WR samples, but the WR-residue differences do not exceed ~0.2‰ in individual xenoliths (Fig. 7a) and are principally within analytical uncertainty.

The leachates in six out of seven samples have significantly lower, and more variable, $\delta^{44/40}$Ca (0.17–0.68‰) than the WR samples and residues (Fig. 7a). The averages for the CaO-rich and Mg,Fe-rich leachates are very close (0.41‰ vs. 0.49‰). A single outlier is leachate from sample 43-86 that yielded anomalously high $\delta^{44/40}$Ca, 1.47 ± 0.03‰ (2sd, n = 3) and 1.46 ± 0.08‰ (2sd, n = 3) for two duplicates (Table 3), much higher than for the residue and WR sample. The Ca isotopic data for the leachate appear to be robust based on good reproducibility of the duplicated analyses, but the reasons for the anomalous values are not clear and are not further discussed below.

As shown in Table 3, the leached fractions account for only 3–12 wt.% Ca in each xenolith, such that the carbonates (with highly variable $\delta^{44/40}$Ca values) appear to have limited influence on $\delta^{44/40}$Ca of the WR samples. Like Sr and Nd isotope ratios, the $\delta^{44/40}$Ca of the residues are negatively correlated with those of the leachates (Fig. 8a).

5. DISCUSSION

5.1 Major element composition and origin of leached carbonate materials

Electron probe analyses of carbonates in our samples (Ionov et al., 1996) show that the dolomite contains 28–40 wt.% CaO, 13–24 wt.% MgO and 0.3–5.0 wt.% FeO while the Mg-calcite contains 44–53 wt.% CaO, 3–11 wt.% MgO and 0.3–2.7 wt.% FeO. The leachates from three xenoliths that host large mosaic carbonate aggregates (4-36-90, 4-90-9 and 21-6) contain 21–33 wt.% CaO, 12–20% MgO and 2.2–3.4% FeO, with higher CaO than for MgO in each case. The leachates from these xenoliths appear to be derived essentially from the dolomite and Mg-calcite in such aggregates.

The leachate from sample 43-86 (that also has large pockets of mosaic Mg-calcite and dolomite) has less CaO (20 wt.%) than MgO (27 wt.%) and thus contains inputs from other carbonate materials. Leachates from the other three xenoliths (63-90-18, SB-4 and 28B) contain even less CaO (9–15 wt.%) and two to four times more MgO (34–37 wt.%) as well as 11–14 wt.% FeO. These ranges correspond to mixtures of dolomite and Mg-calcite with magnesite, ankerite [$Ca(Fe,Mg)(CO_3)_2$] and amorphous carbonate materials at margins of primary carbonate aggregates (Ionov et al., 1993).

Two formation modes could be envisaged for these materials. (1) Reaction of carbonate-rich melts with host peridotites at conditions (e.g. temperature increase related to basaltic magmatism) that do not allow precipitation of coarse Ca-rich carbonates. (2) Recrystallisation and alteration at margins of granular carbonate pockets. While they do not appear to be contaminated by host basalt or post-eruption alteration (that precipitates pure calcite), their composition may not be identical to that of granular metasomatic carbonates.

5.2 'Carbonatite' signatures and residence of Ca, Sr and Nd in WR peridotites

Substantial differences between trace element patterns of leachates and bulk-rocks are seen in Figs. 3–5. The leachates show much greater enrichments of highly incompatible relative to moderately incompatible elements and negative HFSE anomalies, i.e. show essential features inferred for carbonatite metasomatism (e.g. Hauri et al., 1993; Rudnick et al., 1993) that are absent in the bulk-rocks. In particular, WR Type-1 peridotites and residues show no significant Ti-Zr-Hf anomalies and no fractionated Zr/Hf ratios while LREE/HREE ratios are much lower than in the leachates. These results reinforce the conjecture of Ionov et al. (2002a) that element patterns of Spitsbergen peridotites produced by percolation of volatile-bearing mafic melts are not as fractionated as in inferred media of carbonatite metasomatism.

In a more general sense this study suggests that enrichments by volatile-bearing silicate melts, on their own, are not likely to yield chemical signatures typical of

carbonatite metasomatism that require inputs from particular, carbonate-rich liquids. Further, the metasomatic effects of carbonate-rich liquids are less apparent in fertile lherzolites and previously enriched mantle than in highly melt-depleted protoliths (harzburgites, dunites) low in incompatible elements (e.g. Yaxley et al., 1998). The latter is the case for the Spitsbergen samples in which the patterns of bulk-rocks and leached residues are not very different in spite of the presence of carbonates.

The contribution of carbonates to the WR balance of Ca, Sr and Nd and their isotopic ratios in Spitsbergen xenoliths is evaluated here quantitatively from leaching data. Table 3 presents WR Ca-Sr-Nd isotopic compositions calculated from mass proportions of acid-leached material and residues in WR xenoliths, their Ca-Sr-Nd abundances, and $\delta^{44/40}$Ca, ^{87}Sr/^{86}Sr and ^{143}Nd/^{144}Nd values (see also S-Tables 1-2 and Fig. 7). The measured WR compositions are similar to the estimates for the majority of the samples suggesting that the procedure is robust. The only outlier is sample 4-36-90, with the calculated WR ^{87}Sr/^{86}Sr value lower that the measured (Fig. 7b). This may be due to irregular carbonate distribution in the rocks, hence different carbonate mass fractions in the WR powder and sample duplicate used for leaching.

Significant differences in $\delta^{44/40}$Ca were found between the leachates (dissolved carbonates) and leaching residues (silicates), with $\Delta^{44/40}\mathrm{Ca}_{\mathrm{leachate\text{-}residue}}$ from –0.83 to –0.17‰ for six xenoliths, and 0.69‰ for anomalous sample 43-86 (Fig. 7a). By contrast, the WR $\delta^{44/40}$Ca values are within analytical uncertainty (~0.1‰) of those in the residues, indicating small effects of carbonates on $\delta^{44/40}$Ca of the WR xenoliths because of low Ca mass fractions hosted by the carbonates (3–12%; Table 3).

The relations between WR samples, leachates and residues are different for Sr and its isotope ratios. The leachates contain much more Sr than the residues (277–2923 vs. 16–60 ppm; S-Table 2) and have higher ^{87}Sr/^{86}Sr ratios in all the xenoliths. As a result, ^{87}Sr/^{86}Sr in the WR samples are significantly higher than in the residues, in particular for samples 4-36-90, 4-90-9 and 21-6 (cf. Fig. 7b). The leachates from these samples, with carbonates dominated by dolomite and Mg-calcite, have 2337–2923 ppm Sr

(35–51% of Sr mass in WR samples) with $^{87}Sr/^{86}Sr$ ratios of 0.7136–0.7141. Therefore, in spite of the low mass fractions of the leached carbonates in the xenoliths (0.6–1.4%), they host a large share of Sr (8–51 wt.%) and greatly influence $^{87}Sr/^{86}Sr$ ratios in WR peridotites.

The limited Nd isotope data from leaching experiments show that $^{143}Nd/^{144}Nd$ in leachates are close to, or slightly lower, than in residues and WR samples (Fig. 7c), in line with low Nd fractions hosted by carbonates (1–7 wt.%).

To sum up, the role of carbonates is very different in the WR balance of Ca, Sr and Nd abundances and isotopic compositions of Spitsbergen xenoliths. The metasomatic carbonates have very high Sr content and moderate to high $^{87}Sr/^{86}Sr$ ratios, and thus may greatly affect the WR [Sr] and $^{87}Sr/^{86}Sr$ values of mantle peridotites even at low mass fractions. These effects are the greatest for xenoliths with large, unaltered aggregates of dolomite and Mg-calcite.

These observations may help to trace metasomatic history also of some carbonate-free rocks. Carbonates are not stable in the uppermost mantle, and are transient phases rapidly consumed by reaction with orthopyroxene and spinel to form clinopyroxene and olivine (Brey et al., 1983; Dalton and Wood, 1995). This is why carbonates are very rare in mantle xenoliths. As the carbonates react out, Sr enrichments with high $^{87}Sr/^{86}Sr$ ratios, initially residing in carbonates, may ultimately be hosted by clinopyroxene, amphibole, silicate glass, alkali feldspar, phosphates etc.; minerals replacing the carbonates may be zoned and/or include different generations (e.g. Aulbach et al., 2011; Coltorti et al., 1999; Deng et al., 2017; Guo et al., 2020; Ionov et al., 2006; Liu et al., 2012). As a result, unusually high Sr content and isotope ratios in carbonate-free peridotites and their minerals can be seen as indices of metasomatism by carbonate-rich melts that lost CO_2 due to reaction with host mantle. Such reasoning was used by Hauri et al. (1993) to infer hotspot-related carbonatite metasomatism in the oceanic upper mantle based on clinopyroxene analyses. This study provides direct evidence for enrichment of the mantle in radiogenic Sr by

carbonate-rich media.

5.3 Sr isotope evidence for distinct silicate and carbonatite metasomatic media

The Sr isotope data on carbonates in the Spitsbergen xenoliths allow to elucidate the nature of their parental media. The $^{87}Sr/^{86}Sr$ ratios of carbonate-bearing xenoliths, and in particular of leachates (i.e. carbonates) from these samples, are higher than those for leached residues as well as for silicate minerals separated from Spitsbergen xenoliths reported by Ionov et al. (2002b). The differences between the leachates and the silicates are the greatest for three xenoliths with large aggregates of dolomite and Mg-calcite (Fig. 7b; S-Fig. 2a), i.e. the samples apparently most affected by putative carbonate-rich media and least affected by carbonate alteration during eruption. The $^{87}Sr/^{86}Sr$ range (0.7136–0.7141) in the leachates from these samples may be close to $^{87}Sr/^{86}Sr$ in these media. This unequivocally demonstrates the lack of Sr isotope equilibrium between the carbonates on the one hand, and coarse silicates in these xenoliths on the other hand. This further implies that the carbonates could not be formed from the liquids that metasomatized the silicate minerals because in such a case the carbonates and the silicates would have very similar $^{87}Sr/^{86}Sr$ ratios. We see this is as a definitive proof that the carbonates were formed from a distinct carbonate-rich liquid unrelated to silicate metasomatism.

High $^{87}Sr/^{86}Sr$ (~0.714) in metasomatic media require high long-term Rb/Sr ratios in their sources, e.g. due to high modal phlogopite or K-amphibole. High $^{87}Sr/^{86}Sr$ were reported for clinopyroxene and amphibole from MARID xenoliths (0.705–0.936 Fitzpayne et al., 2019; Kramers et al., 1983), carbonate mantle xenoliths (~0.709 Howarth et al., 2019) and pyroxenites from North China (up to 0.715 Dai et al., 2020). Such domains may form in the mantle by fractionation of melts, e.g. at the top of a mantle plume, or more likely by incorporation of (a) blocks delaminated from the base of mantle lithosphere or (b) subducted crustal materials. For instance, Hauri et al. (1993) attributed high $^{87}Sr/^{86}Sr$ (up to 0.713) in clinopyroxene in mantle xenoliths

from the Pacific to 'carbonatite' metasomatism by melts derived from recycled crustal components in the convecting mantle. Our data do not allow to distinguish mantle vs. crustal origins for the radiogenic Sr in the xenoliths in this study.

The very broad $^{87}Sr/^{86}Sr$ range (0.7049–0.7141) of the leachates (i.e. carbonates), along with covariation of $^{87}Sr/^{86}Sr$ in the leachates and the residues (Fig. 8b) indicate some limited isotope exchange between the carbonate-rich melt and host peridotites. The exchange may have continued during or after the formation of the carbonates, in particular for interstitial carbonate aggregates with greater surface relative to mass (S-Fig. 1b-c, EA2). This may be the reason why the carbonate-rich melts (and/or initially deposited dolomite and Mg-calcite in such pockets) reacted to form late-stage, Mg-Fe-rich carbonates common in many xenoliths in this study (S-Fig. 1G).

To sum up, we posit that granular dolomite and Mg-calcite formed from a parental carbonate-rich liquid that had $^{87}Sr/^{86}Sr$ of ~0.714. The liquid, and possibly the initial carbonates, reacted with the host peridotites ($^{87}Sr/^{86}Sr$ ~ 0.7025–0.7041; Ionov et al. (2002b)) to form late-stage Mg-Fe carbonates. Sr-isotope exchange between the carbonate-rich melt and host rocks increased the $^{87}Sr/^{86}Sr$ ratios in host peridotites, the more so in the samples with more carbonates, and produced the positive correlation of $^{87}Sr/^{86}Sr$ in leachates and residues, i.e. coexisting silicates and carbonates (Fig. 8b).

The $^{87}Sr/^{86}Sr$ ratios in the residues of leaching that removed carbonates from the Spitsbergen xenoliths (0.7036–0.7055) are higher than in the depleted MORB mantle (DMM, ~0.7025; Fig. 6a) (e.g. Carlson and Ionov, 2019; Stracke, 2012). This can be best explained by an earlier episode of 'silicate' metasomatism and possibly later exchanges with evolving carbonate-rich melts (see above).

Late-stage metasomatism taking place shortly before volcanic eruptions that bring mantle fragments to the surface has been documented in many xenolith suites. Remarkable examples of this phenomenon are xenoliths containing pockets and veins of silicate glass (e.g. Coltorti et al., 1999; Ionov et al., 1994), usually attributed to pre-eruption intrusion of carbonate-rich media, as well as sheared cratonic peridotites

with deformation accompanying melt metasomatism (e.g. Agashev et al., 2013; Ionov et al., 2017; Katayama et al., 2009; van der Meer et al., 2013). Geophysical and experimental data (e.g. Xu et al., 2020) suggest that low-volume carbonate-rich melts can be pervasively present in the deep upper mantle. Such melts may trail upwelling mantle that generates xenolith-bearing magmas and react with their wall-rocks.

5.4 Ca isotope fractionation in the Spitsbergen mantle

Radiogenic ^{40}Ca enrichment from ^{40}K decay can decrease $\delta^{44/40}$Ca values in rocks with old ages and high K/Ca ratios (Fantle and Tipper, 2014). The lithospheric mantle beneath Spitsbergen apparently formed in early Paleoproterozoic, most likely between 1.7 and 2.7 Ga based on Lu-Hf and Re-Os isotope data (Choi et al., 2010). However, WR samples and residues in this study have low K/Ca ratios (<0.03; S-Table 1) such that ^{40}K decay could decrease $\delta^{44/40}$Ca of any of these samples only by <0.02‰, i.e. within analytical uncertainties, and thus could not affect the observed $\delta^{44/40}$Ca range.

As noted in Section 2, the Al_2O_3 range in the Spitsbergen xenoliths indicates that their protoliths were residues of melt extraction (Ionov et al., 2002a) because Al_2O_3 in mantle rocks is a robust melting index, little affected by metasomatism (Pearson et al., 2014). Peridotites formed by melt extraction from fertile mantle and unaffected by posterior metasomatism, like those from Tariat in Mongolia (Carlson and Ionov, 2019; Ionov and Hofmann, 2007), define linear co-variation on CaO vs. Al_2O_3 plots (Fig. 1a), that overlaps the primitive mantle (PM) (McDonough and Sun, 1995). Some Spitsbergen peridotites plot close to this trend, but many have higher CaO and Ca/Al ratios at given Al_2O_3 (Fig. 1a, b) indicating post-melting Ca enrichments. These enrichments are partly hosted by carbonates, but the fact that six out of seven leached residues show higher CaO and Ca/Al ratios than the melt-extraction trend (Fig. 1a, b) suggest that metasomatic Ca additions may be mainly hosted by silicates. Overall, the Ca budget in the Spitsbergen xenoliths records the combined effects of melt extraction and enrichments by silicate and carbonatite media.

5.4.1 $\delta^{44/40}$Ca in products of melting and silicate metasomatism

Recent studies found that large degrees of partial melting may induce small, but conspicuous Ca isotopic fractionation, with higher $\delta^{44/40}$Ca in refractory melting residues than in coexisting melts. This inference is supported, first, by data on fertile to refractory mantle peridotites that show: (a) co-variation of $\delta^{44/40}$Ca with Al_2O_3 and CaO (Fig. 9a-b); (b) higher (by ~0.1‰) than in the BSE estimate $\delta^{44/40}$Ca values for melt-depleted (and non-metasomatized, i.e. LREE-depleted) low-Ca-Al lherzolites and harzburgites (e.g. Ionov et al., 2019; Kang et al., 2017). Furthermore, oceanic basalts show $\delta^{44/40}$Ca values that are consistently lower than in the BSE, e.g. 0.83 ± 0.11‰ (2sd, n = 21) for MORB and 0.80 ± 0.08‰ (2sd, n = 21) for back-arc basin basalts (Chen et al., 2020; Zhu et al., 2020; Zhu et al., 2018b).

Chen et al. (2019) obtained average $\delta^{44/40}$Ca of 0.94 ± 0.11‰ (2sd, n = 22) for melt-depleted (2.0–3.4 wt.% Al_2O_3) lherzolites from two tectonically emplaced massifs in the Alps. They failed to establish correlations of $\delta^{44/40}$Ca with Al_2O_3 (i.e. melting degrees), apparently because of the lack of fertile lherzolites and complex melt impregnation in their samples. Furthermore, they reported $\delta^{44/40}$Ca below the BSE estimate both in residual harzburgites (0.89 ± 0.09‰; 2sd, n = 3) and magmatic pyroxenites (0.86 ± 0.10‰; 2sd, n = 14). We find confusing that Chen et al. (2019) used their data to define the $\delta^{44/40}$Ca range, alternately, for "Earth's mantle", "upper mantle" or "fertile mantle rocks" as 0.94 ± 0.10‰ (2sd, n = 47). The Earth's mantle is heterogeneous, with $\delta^{44/40}$Ca well beyond the above range reported both for xenoliths of the lithospheric mantle (e.g. Chen et al., 2018; Ionov et al., 2019; Kang et al., 2019; Kang et al., 2020)) and asthenosphere-derived magmatic rocks (see above). Further, the above range cannot refer to "fertile mantle" because Chen et al. (2019) reported data on melt-depleted peridotites overprinted by melt infiltration (without trace element data to evaluate possible metasomatic inputs).

The Al_2O_3 content in leached residues in this study is much lower than in the BSE

(1.30–2.45 vs. 4.45 wt.%; McDonough and Sun (1995)) indicating that they experienced ~10–25% of partial melting (Herzberg, 2004). The $\delta^{44/40}$Ca values of melting residues with this Al_2O_3 range should be ~0.12–0.04‰ higher than in the BSE based on equilibrium fractionation modeling (Fig. 9a-b Chen et al., 2019; Kang et al., 2017). By contrast, the $\delta^{44/40}$Ca values for six out of seven leached samples (0.78–0.90‰, av. 0.83 ± 0.09‰, 2sd) and 16 out of 17 WR Spitsbergen samples (0.73–0.89‰, av. 0.83 ± 0.10‰, 2sd) are lower than the BSE estimate (0.94 ± 0.05‰; Kang et al. (2017)) and for non-metasomatized (from trace element data) fertile and melt-depleted peridotites in the literature (Fig. 9). The $\delta^{44/40}$Ca values in the majority of the Spitsbergen samples are below the BSE range also if the uncertainty of individual analyses is considered (Fig. 9). We conclude that the silicate metasomatism decreased $\delta^{44/40}$Ca values in the Spitsbergen lithospheric mantle by 0.1–0.2‰ relative to the likely range of ~1.0–1.1‰ in the initial melting residues (e.g. Kang et al., 2017).

Earlier xenolith studies inferred that metasomatism by silicate melts may decrease $\delta^{44/40}$Ca in fertile or melt-depleted peridotites (e.g. Kang et al., 2017), but its effects on Ca isotopes continue to be debated. Kang et al. (2019) reported low $\delta^{44/40}$Ca values (0.65–0.87‰), correlated with $(Gd/Yb)_N$, for Ca-Fe-rich lherzolites and wehrlites from Tok in the SE Siberian craton formed by reaction of lherzolites and harzburgites with silica-undersaturated partial melts. Kang et al. (2019) used equilibrium isotope fractionation modeling to infer that the Tok mantle was metasomatized by low-$\delta^{44/40}$Ca liquids generated from eclogites. The $\delta^{44/40}$Ca values of leached Spitsbergen xenoliths are not correlated with $(Gd/Yb)_N$, which argues against metasomatism by silicate melts from eclogite-rich sources. We see no reason to link these values to kinetic fractionation (e.g. Zhao et al., 2017) either because our samples show no modal or chemical (e.g. Fe enrichments) heterogeneities indicative of such a process.

Overall, the $\delta^{44/40}$Ca range in the leaching residues, hence in the Spitsbergen mantle before the most recent enrichment event, can be explained by a combination of melt

extraction, that moderately increased $\delta^{44/40}$Ca values, and subsequent silicate-melt metasomatism that brought $\delta^{44/40}$Ca in the melting residues below the BSE range.

5.4.2 Carbonatite Metasomatism

The effects of carbonatite metasomatism on $\delta^{44/40}$Ca of mantle peridotites can be directly evaluated using data on carbonate-bearing xenoliths. Ionov et al. (2019) reported leaching data on xenoliths from the Obnazhennaya (Obn) kimberlite on the NE Siberian craton that contain carbonates texturally equilibrated with silicates. The $\delta^{44/40}$Ca values in leachates from these samples (0.82–0.84‰) are similar to those for leached residues (0.70–0.84‰) within analytical uncertainty, which Ionov et al. (2019) attributed to Ca isotope equilibration of the carbonates with silicates (Fig. 8a).

By contrast, the carbonates in the Spitsbergen xenoliths mainly occur in texturally discordant pockets and veins, and differ strongly in Ca and Sr isotopic compositions from the leached silicate residues (Fig. 7). These carbonates are usually enclosed in Na,Al-rich silicate glass and fine-grained aggregates of silicates and spinel formed by reaction of carbonate-rich melts with host mantle (Ionov, 1998; Ionov et al., 1996), i.e. are out of chemical equilibrium with coarse silicates and have little direct contact with them. This, together with the short duration of the melt-rock reaction, may explain why the parental carbonate-rich melts did not attain Ca-Sr isotope equilibrium with the host mantle. The broad ranges of $\delta^{44/40}$Ca (0.17–0.68‰) and ^{87}Sr/^{86}Sr (0.7049–0.7141) in the leachates may be related to different amounts of the carbonate-rich melts and extents of isotopic exchange with host peridotites.

The differences between $\delta^{44/40}$Ca values of bulk (0.73–0.95‰) and leached (0.78–1.00‰) Spitsbergen xenoliths (Figs. 6a and 7a) are minor and imply limited bulk contributions from carbonatite metasomatism. This observation is consistent with Ca-isotope data on relevant mantle rocks from the literature. The $\delta^{44/40}$Ca values in the majority of carbonate-bearing Obn xenoliths are only 0.10–0.15‰ lower than the BSE estimate (Fig. 9; Ionov et al. (2019). Few mantle xenoliths presumably affected

by carbonatite metasomatism reported in Ionov et al. (2019) and Kang et al. (2017) deviate by >0.3‰ from the BSE estimate. The greatest metasomatism-induced Ca isotope effects are found in rocks with low pre-metasomatic Ca content that had high Ca additions and developed high Ca/Al ratios. Mass balance estimates show that the carbonates only account for 3–12% of Ca in the WR Spitsbergen xenoliths (Table 3), in line with the relatively low Ca/Al ratios (<2) in these xenoliths (Fig. 9c).

To sum up, both carbonatite and silicate metasomatism reduced $\delta^{44/40}$Ca values of Spitsbergen peridotites and thus contributed to Ca isotope mantle heterogeneity. Both processes may result in lower $\delta^{44/40}$Ca values in mantle peridotites than in the BSE or melting residues such that Ca isotopes cannot robustly distinguish between these two types of mantle metasomatism (Ionov et al., 2019). On the other hand, the very low $\delta^{44/40}$Ca in acid-leached materials from some carbonate-bearing Spitsbergen xenoliths, together with literature data on refractory peridotites with high Ca/Al, indicate that carbonatite metasomatism has a potential to yield the lowest $\delta^{44/40}$Ca in the mantle.

5.5 Sources of carbonatites and carbonate-rich media of mantle metasomatism

The isotopic signatures of metasomatism in the lithospheric mantle are related to the nature and sources of its media. An important issue is the share of carbonates in such media. Early experimental data and studies of mantle xenoliths evoked sodic dolomitic carbonate melts (e.g. Yaxley et al., 1991) while studies of CO_2-rich magmas (carbonatites and kimberlites) suggest that near-solidus melts of carbonated peridotite must be silicate-dominated with only dilute carbonate contents (e.g. Tappe et al., 2017). Furthermore, discrete CO_2-rich magma batches with different $\delta^{44/40}$Ca ratios may be derived from mixed sources in the convecting upper mantle (Tappe et al., 2020). The common association of carbonates in the Spitsbergen xenoliths with silicate glass and fine-grained silicates suggest that their parental liquids contain silicate components, but their share cannot be constrained from our data.

Carbonate-rich liquids generated both from ‘juvenile’ carbonated mantle and

sources containing subducted carbonates were recently evoked to explain the origin of carbonatites and kimberlites (e.g. Banerjee and Chakrabarti, 2019; Tappe et al., 2017). Ionov et al. (2019) argued that recycling of carbonates, that show a broad $\delta^{44/40}$Ca range, may not always alter the Ca isotopic composition in global mantle. Banerjee and Chakrabarti (2019) reported a $\delta^{44/40}$Ca range of 0.6–1.1‰, that overlaps the BSE estimate, for seven carbonatites from India and explained it by mixing of the plume end-member with recycled carbonates. Amsellem et al. (2020) obtained a much lower average $\delta^{44/40}$Ca = 0.26 ± 0.25‰ (2 sd, n = 50) for Ca-Mg-Fe carbonatites and argued that it reflects the incorporation of isotopically light marine carbonates into their mantle sources. By contrast, Sun et al. (2021) reported primary carbonatite and associated silicate rocks that are rather homogeneous in Ca isotope compositions that are comparable to those of basalts, which implies that the carbonatites are generated from a 'juvenile' mantle source without requiring the involvement of recycled carbonates. Banerjee et al. (2021) found BSE-like $\delta^{44/40}$Ca values in carbonatites older than 0.3 Ga, but low $\delta^{44/40}$Ca values (0.63‰, n=29) in younger carbonatites. While the topic may require further investigation, it is evident that carbonate-rich mantle melts may have both BSE-like and low $\delta^{44/40}$Ca values. This is consistent with inferences in this study that Ca isotope data cannot robustly distinguish carbonate and silicate mantle metasomatism (see the previous section).

This study found lower $\delta^{44/40}$Ca than for the BSE in the carbonates of mantle origin in Spitsbergen xenoliths. It appears that carbonatite metasomatism generally lowers $\delta^{44/40}$Ca in mantle rocks, likely including basalt source regions (Huang et al., 2011; Ionov et al., 2019; Kang et al., 2017; Kang et al., 2016; Liu et al., 2017a). However, the limited available data also suggest that carbonatite metasomatism may not change $\delta^{44/40}$Ca in the lithospheric mantle very much, except for rare highly refractory peridotites (Ionov et al., 2019), the latter are insignificant in mantle magma sources.

6. SUMMARY OF CONCLUSIONS

Leaching of peridotite xenoliths from Spitsbergen with acetic acid extracted carbonates formed in the latest metasomatic event and thus allowed to distinguish chemical and Ca-Sr-isotope imprints of their parental carbonate-rich melts from the combined effects of melt extraction and silicate metasomatism in leaching residues.

PM-normalized trace element patterns of the leached carbonates, unlike silicate residues, show distinctive indices (LREE-enrichments, HFSE-depletions) of carbonatite mantle metasomatism, suggesting that it necessitates specific carbonate-rich liquids rather than fractionation products of volatile-bearing silicate melts.

The carbonates are out of Ca-Sr isotope equilibrium with the silicates in the Spitsbergen peridotites implying that the silicate and carbonatite metasomatism are produced by different parental melts from distinct sources. This proves the existence of distinctive carbonate-rich metasomatic media in the lithospheric mantle.

The Spitsbergen carbonates are rich in Sr (277–2923 ppm) and have high $^{87}Sr/^{86}Sr$ (0.7049–0.7141). These signatures are retained in host peridotites when the transient carbonates react out to form Ca-rich silicates. High [Sr] and $^{87}Sr/^{86}Sr$ may be indices (though not definitive proofs) of carbonatite metasomatism in mantle rocks.

The ranges of $^{87}Sr/^{86}Sr$ (0.7136–0.7141) and $\delta^{44/40}Ca$ (0.35–0.45‰) in leachates from three peridotites with large aggregates of dolomite and Mg-calcite constrain their values in sources of putative carbonate-rich media that either had high long-term Rb/Sr ratios or included recycled materials.

Both carbonatite and silicate metasomatism may produce $\delta^{44/40}Ca$ values lower than the BSE, such that that Ca-isotope data cannot robustly tell apart these two enrichment types, yet carbonatite metasomatism may yield the lowest $\delta^{44/40}Ca$.

ACKNOWLEDGEMENTS

We are grateful to Yajun An, Fang Liu, Jinting Kang, Jianghao Bai, Wei Wu and Zebin Luo for help with analyses and discussions. This study was supported by grants from the National

Natural Science Foundation of China (No. 41773009 and 41873002) and the Programme National de Planétologie (PNP) of CNRS/INSU/CNES (grants to DAI in 2018-2019). DAI acknowledges Chinese Academy of Sciences President's International Fellowship Initiative (PIFI) for Visiting Scientists in 2019 (Grant No. 2017VCA0009). We appreciate constructive comments of S. Aulbach, S. Tappe, two anonymous reviewers and AE (A. Stracke).

Figure Captions

Fig. 1. Co-variation plots for (a) CaO (wt.%), (b) Ca/Al ratios and (c) Sr (ppm) versus Al_2O_3 (wt.%) in whole rock (WR) peridotite xenoliths from Spitsbergen (Spi) (Ionov et al., 2002a) and in acid-leached samples of the same xenoliths (this study). Also shown are the primitive mantle (PM, McDonough and Sun, 1995) and WR peridotite xenoliths from Tariat (Tar) in Mongolia (Ionov, 2007; Ionov and Hofmann, 2007) that define a regular melt extraction trend (grey area in (a)), experienced no or little metasomatism after melting, and are similar in composition to depleted MORB mantle (Carlson and Ionov, 2019). Some Spitsbergen peridotites plot above the fields of the Tariat xenoliths due to metasomatic enrichments in Ca and Sr. Both leached and non-leached Spitsbergen xenoliths are enriched in Ca suggesting that much Ca resides in silicates. By contrast, non-leached bulk-rocks contain more Sr than acid-leached xenoliths because the carbonates may host more Sr than silicates.

Fig. 2. Primitive mantle-normalized (McDonough and Sun, 1995) REE (left column) and multi-element abundance patterns for whole-rock Spitsbergen peridotites. Data and rock types are after Ionov et al. (2002a).

Fig. 3. Comparison of trace element concentrations of leachates (Leach), leached residues (Res) and whole rocks (WR) for samples SB-4 and 43-86 in this study with leaching data of the same samples from Ionov et al. (1993) assuming that leached materials make up 1 wt.% of bulk rocks. The inferred element concentrations in the leached materials after Ionov et al. (1993) are much higher because they employed diluted HNO_3, which dissolved not only carbonates as in this study, but also extracted trace elements from silicates.

Fig. 4. Primitive mantle-normalized (McDonough and Sun, 1995) REE patterns

for leachates (Leach) , residues (Res) and whole-rocks (WR) of carbonate-bearing peridotites.

Fig. 5. PM-normalized (McDonough and Sun, 1995) multi-element abundance patterns for leachates, residues and whole-rocks of carbonate-bearing peridotites.

Fig. 6. Plots of $\delta^{44/40}$Ca vs. (a) ^{87}Sr/^{86}Sr and (b) ^{143}Nd/^{144}Nd for leachates (Leach), residues (Res) and whole-rocks (WR) of Spitsbergen xenoliths. The blue horizontal line and grey bar represent the $\delta^{44/40}$Ca estimate for the BSE (Kang et al., 2017). The vertical dashed lines represent ^{87}Sr/^{86}Sr and ^{143}Nd/^{144}Nd for three types of the depleted MORB mantle (DMM): D-DMM, DMM and E-DMM after Workman and Hart (2005).

Fig. 7. Comparisons of (a) $\delta^{44/40}$Ca, (b) ^{87}Sr/^{86}Sr and (c) ^{143}Nd/^{144}Nd in leachates (Leach), residues (Res) and whole-rocks (WR) for seven carbonate-bearing Spitsbergen xenoliths as well as Sr and Nd isotopic ratios of cpx (Ionov et al., 2002b).

Fig. 8. Co-variation plots of $\delta^{44/40}$Ca (a), ^{87}Sr/^{86}Sr (b) and ^{143}Nd/^{144}Nd (c) for leachates and leaching residues in individual xenoliths. from Spitsbergen (Spi). Also shown are leachates and leaching residues in metasomatized, carbonate-bearing Obnazhennaya (Obn) peridotites (Ionov et al., 2019). Thick grey lines represent equal Ca-Sr-Nd isotopic values in leachates and leaching residues.

Fig. 9. Co-variation plots of $\delta^{44/40}$Ca versus wt.% Al_2O_3 (a), wt.% CaO (b) and Ca/Al (c) in WR xenoliths and leaching residues (Res) of Spitsbergen (Spi) xenoliths. Also shown are melt-depleted peridotites from Tariat (Mongolia), and metasomatized, carbonate-bearing Obnazhennaya peridotites (Ionov et al., 2019; Kang et al., 2017). The blue horizontal line and gray bar represent estimated $\delta^{44/40}$Ca of the BSE and 2sd of the BSE estimate (Kang et al., 2017). The $\delta^{44/40}$Ca in the melt-depleted peridotites from Tariat and Obnazhennaya are negatively correlated with Al_2O_3 and CaO. The leached Spitsbergen xenoliths display a negative $\delta^{44/40}$Ca vs. Al_2O_3 correlation, but their $\delta^{44/40}$Ca values are lower than those for non-metasomatized melting residues from the literature.

REFERENCES

Agashev A. M., Ionov D. A., Pokhilenko N. P., Golovin A. V., Cherepanova Y. and Sharygin I. S. (2013) Metasomatism in lithospheric mantle roots: Constraints from whole-rock and mineral chemical composition of deformed peridotite xenoliths from kimberlite pipe Udachnaya. *Lithos* **160–161**, 201-215.

Amini M., Eisenhauer A., Böhm F., Holmden C., Kreissig K., Hauff F. and Jochum Klaus P. (2009) Calcium Isotopes (δ 44/40Ca) in MPI - DING Reference Glasses, USGS Rock Powders and Various Rocks: Evidence for Ca Isotope Fractionation in Terrestrial Silicates. *Geostand. Geoanal. Res.* **33**, 231-247.

Amsellem E., Moynier F., Bertrand H., Bouyon A., Mata J., Tappe S. and Day J. M. D. (2020) Calcium isotopic evidence for the mantle sources of carbonatites. *Science Advances* **6**, eaba3269.

Antonelli M. A. and Simon J. I. (2020) Calcium isotopes in high-temperature terrestrial processes. *Chem. Geol.* **548**, 119651.

Aulbach S., Rudnick R. L. and McDonough W. F. (2011) Evolution of the lithospheric mantle beneath the East African Rift in Tanzania and its potential signatures in rift magmas. *Geol. Soc. Am. Spec. Pap.* **478**, 105-125.

Banerjee A. and Chakrabarti R. (2019) A geochemical and Nd, Sr and stable Ca isotopic study of carbonatites and associated silicate rocks from the ~65 Ma old Ambadongar carbonatite complex and the Phenai Mata igneous complex, Gujarat, India: Implications for crustal contamination, carbonate recycling, hydrothermal alteration and source-mantle mineralogy. *Lithos* **326-327**, 572-585.

Banerjee A., Chakrabarti R. and Simonetti A. (2021) Temporal evolution of δ44/40Ca and 87Sr/86Sr of carbonatites: Implications for crustal recycling through time. *Geochim. Cosmochim. Acta* **307**, 168-191.

Blättler C. L. and Higgins J. A. (2017) Testing Urey's carbonate–silicate cycle using the calcium isotopic composition of sedimentary carbonates. *Earth Planet Sci Lett* **479**, 241-251.

Bodinier J.-L., Vasseur G., Vernières J., Dupuy C. and Fabriès J. (1990) Mechanisms of mantle metasomatism: geochemical evidence from the Lherz orogenic peridotite. *J. Petrol.* **31**, 597-628.

Brey G., Brice W. R., Ellis D. J., Green D. H., Harris K. L. and Ryabchikov I. D. (1983) Pyroxene-carbonate reactions in the upper mantle. *Earth Planet Sci Lett* **62**, 63-74.

Carlson R. W. and Ionov D. A. (2019) Compositional characteristics of the MORB mantle and bulk silicate earth based on spinel peridotites from the Tariat Region, Mongolia. *Geochim. Cosmochim. Acta* **257**, 206-223.

Charlier B. L. A., Ginibre C., Morgan D., Nowell G. M., Pearson D. G., Davidson J. P. and Ottley C. J. (2006) Methods for the microsampling and high-precision analysis of strontium and rubidium isotopes at single crystal scale for petrological and geochronological applications. *Chem. Geol.* **232**, 114-133.

Chen C., Ciazela J., Li W., Dai W., Wang Z., Foley S. F., Li M., Hu Z. and Liu Y. (2020)

Calcium isotopic compositions of oceanic crust at various spreading rates. *Geochim. Cosmochim. Acta* **278**, 272-288.

Chen C., Dai W., Wang Z., Liu Y., Li M., Becker H. and Foley S. F. (2019) Calcium isotope fractionation during magmatic processes in the upper mantle. *Geochim. Cosmochim. Acta* **249**, 121-137.

Chen C., Liu Y., Feng L., Foley S. F., Zhou L., Ducea M. N. and Hu Z. (2018) Calcium isotope evidence for subduction-enriched lithospheric mantle under the northern North China Craton. *Geochim. Cosmochim. Acta* **238**, 55-67.

Choi S. H., Suzuki K., Mukasa S. B., Lee J.-I. and Jung H. (2010) Lu-Hf and Re-Os systematics of peridotite xenoliths from Spitsbergen, western Svalbard: Implications for mantle-crust coupling. *Earth Planet Sci Lett* **297**, 121-132.

Coltorti M., Bonadiman C., Hinton R. W., Siena F. and Upton B. G. J. (1999) Carbonatite metasomatism of the oceanic upper mantle: Evidence from clinopyroxenes and glasses in ultramafic xenoliths of Grande Comore, Indian Ocean. *J. Petrol.* **40**, 133-165.

Dai W., Wang Z., Liu Y., Chen C., Zong K., Zhou L., Zhang G., Li M., Moynier F. and Hu Z. (2020) Calcium isotope compositions of mantle pyroxenites. *Geochimica et Cosmochimica Acta* **270**, 144-159.

Dalton J. A. and Wood B. J. (1995) The stability of carbonate under upper-mantle conditions as a function of temperature and oxygen fugacity. *Eur. J. Miner.* **7**, 883-891.

Dautria J. M., Dupuy C., Takherist D. and Dostal J. (1992) Carbonate metasomatism in the lithospheric mantle: the peridotitic xenoliths from a melilititic district of the Sahara Basin. *Contrib. Mineral. Petrol.* **111**, 37-52.

Deng L., Liu Y., Zong K., Zhu L., Xu R., Hu Z. and Gao S. (2017) Trace element and Sr isotope records of multi-episode carbonatite metasomatism on the eastern margin of the North China Craton. *Geochem. Geophys. Geosyst.* **18**, 220-237.

DePaolo D. J. (2004) Calcium Isotopic Variations Produced by Biological, Kinetic, Radiogenic and Nucleosynthetic Processes. *Rev. Mineral. Geochem.* **55**, 255-288.

Du L., Long X., Yuan C., Zhang Y., Huang Z., Sun M. and Xiao W. (2018) Petrogenesis of Late Paleozoic diorites and A-type granites in the central Eastern Tianshan, NW China: Response to post-collisional extension triggered by slab breakoff. *Lithos* **318-319**, 47-59.

Du L., Yuan C., Li X.-P., Zhang Y., Huang Z. and Long X. (2019) Petrogenesis and Geodynamic Implications of the Carboniferous Granitoids in the Dananhu Belt, Eastern Tianshan Orogenic Belt. *J. Earth Sci.* **30**, 1243-1252.

Fantle M. S. and Tipper E. T. (2014) Calcium isotopes in the global biogeochemical Ca cycle: Implications for development of a Ca isotope proxy. *Earth-Sci. Rev.* **129**, 148-177.

Farkaš J., Böhm F., Wallmann K., Blenkinsop J., Eisenhauer A., van Geldern R., Munnecke A., Voigt S. and Veizer J. (2007) Calcium isotope record of Phanerozoic oceans: Implications for chemical evolution of seawater and its causative mechanisms. *Geochim. Cosmochim. Acta* **71**, 5117-5134.

Feng L.-p., Zhou L., Yang L., DePaolo D. J., Tong S.-Y., Liu Y.-S., Owens T. L. and Gao S. (2017) Calcium Isotopic Compositions of Sixteen USGS Reference Materials. *Geostand. Geoanal. Res.* **41**, 93-106.

Fitzpayne A., Giuliani A., Maas R., Hergt J., Janney P. and Phillips D. (2019) Progressive metasomatism of the mantle by kimberlite melts: Sr–Nd–Hf–Pb isotope compositions of MARID and PIC minerals. *Earth and Planetary Science Letters* **509**, 15-26.

Frezzotti M. L., Andersen T., Neumann E.-R. and Simonsen S. L. (2002) Carbonatite melt-CO_2 fluid inclusions in mantle xenoliths from Tenerife, Canary Islands: a story of trapping, immiscibility and fluid-rock interaction in the upper mantle. *Lithos* **64**, 77-96.

Green D. H. and Wallace M. E. (1988) Mantle metasomatism by ephemeral carbonatite melts. *Nature* **336**, 459-462.

Griffin W. L., Nikolic N., O'Reilly S. Y. and Pearson N. J. (2012) Coupling, decoupling and metasomatism: Evolution of crust–mantle relationships beneath NW Spitsbergen. *Lithos* **149**, 115-135.

Guo P., Ionov D. A., Xu W.-L., Wang C.-G. and Luan J.-P. (2020) Mantle and recycled oceanic crustal components in mantle xenoliths from northeastern China and their mantle sources. *J. Geophys. Res. Solid Earth* **125**, e2019JB018232.

Hauri E. H., Shimizu N., Dieu J. J. and Hart S. R. (1993) Evidence for hotspot-related carbonatite metasomatism in the oceanic upper mantle. *Nature* **365**, 221-227.

He Y., Wang Y., Zhu C., Huang S. and Li S. (2017) Mass-Independent and Mass-Dependent Ca Isotopic Compositions of Thirteen Geological Reference Materials Measured by Thermal Ionisation Mass Spectrometry. *Geostand. Geoanal. Res.* **41**, 283-302.

Herzberg C. (2004) Geodynamic information in peridotite petrology. *J. Petrol.* **45**, 2507-2530.

Heuser A., Eisenhauer A., Gussone N., Bock B., Hansen B. T. and Nägler T. F. (2002) Measurement of calcium isotopes (δ44Ca) using a multicollector TIMS technique. *Int. J. Mass Spectrom.* **220**, 385-397.

Hofmann A. W. (1988) Chemical differentiation of the Earth: the relationship between mantle, continental crust, and oceanic crust. *Earth Planet Sci Lett* **90**, 297-314.

Hofmann A. W. (1997) Mantle geochemistry: the message from oceanic volcanism. *Nature* **385**, 219-229.

Hofmann A. W. (2003) Sampling mantle heterogeneity through oceanic basalts: isotopes and trace elements, in: Carlson, R.W. (Ed.), Treatise on Geochemistry. Vol. 2. The Mantle and Core. Elsevier, pp. 61-102.

Howarth G. H., Moore A. E., Harris C., van der Meer Q. H. A. and le Roux P. (2019) Crustal versus mantle origin of carbonate xenoliths from Kimberley region kimberlites using C-O-Sr-Nd-Pb isotopes and trace element abundances. *Geochimica et Cosmochimica Acta* **266**, 258-273.

Huang S., Farkas J. and Jacobsen S. B. (2010) Calcium isotopic fractionation between clinopyroxene and orthopyroxene from mantle peridotites. *Earth Planet Sci Lett* **292**, 337-344.

Huang S., Farkaš J. and Jacobsen S. B. (2011) Stable calcium isotopic compositions of Hawaiian shield lavas: Evidence for recycling of ancient marine carbonates into the mantle. *Geochim. Cosmochim. Acta* **75**, 4987-4997.

Ionov D. and Harmer R. E. (2002) Trace element distribution in calcite-dolomite carbonatites from Spitskop: inferences for differentiation of carbonatite magmas and the origin of

carbonates in mantle xenoliths. *Earth and Planetary Science Letters* **198**, 495-510.
Ionov D. A. (1998) Trace element composition of mantle-derived carbonates and coexisting phases in peridotite xenoliths from alkali basalts. *J. Petrol.* **39**, 1931-1941.
Ionov D. A. (2007) Compositional variations and heterogeneity in fertile lithospheric mantle: peridotite xenoliths in basalts from Tariat, Mongolia. *Contrib. Mineral. Petrol.* **154**, 455-477.
Ionov D. A., Bodinier J.-L., Mukasa S. B. and Zanetti A. (2002a) Mechanisms and sources of mantle metasomatism: major and trace element compositions of peridotite xenoliths from Spitsbergen in the context of numerical modeling. *J. Petrol.* **43**, 2219-2259.
Ionov D. A., Doucet L. S., Pogge von Strandmann P. A. E., Golovin A. V. and Korsakov A. V. (2017) Links between deformation, chemical enrichments and Li-isotope compositions in the lithospheric mantle of the central Siberian craton. *Chem. Geol.* **475**, 105-121.
Ionov D. A., Doucet L. S., Xu Y., Golovin A. V. and Oleinikov O. B. (2018) Reworking of Archean mantle in the NE Siberian craton by carbonatite and silicate melt metasomatism: Evidence from a carbonate-bearing, dunite-to-websterite xenolith suite from the Obnazhennaya kimberlite. *Geochimica et Cosmochimica Acta* **224**, 132-153.
Ionov D. A., Dupuy C., O'Reilly S. Y., Kopylova M. G. and Genshaft Y. S. (1993) Carbonated peridotite xenoliths from Spitsbergen: implications for trace element signature of mantle carbonate metasomatism. *Earth Planet Sci Lett* **119**, 283-297.
Ionov D. A. and Hofmann A. W. (2007) Depth of formation of sub-continental off-craton peridotites. *Earth Planet Sci Lett* **261**, 620-634.
Ionov D. A., Hofmann A. W. and Shimizu N. (1994) Metasomatism-induced melting in mantle xenoliths from Mongolia. *J. Petrol.* **35**, 753-785.
Ionov D. A., Mukasa S. B. and Bodinier J.-L. (2002b) Sr-Nd-Pb isotopic compositions of peridotite xenoliths from Spitsbergen: numerical modelling indicates Sr-Nd decoupling in the mantle by melt percolation metasomatism. *J. Petrol.* **43**, 2261-2278.
Ionov D. A., O'Reilly S. Y., Kopylova M. G. and Genshaft Y. S. (1996) Carbonate-bearing mantle peridotite xenoliths from Spitsbergen: phase relationships, mineral compositions and trace element residence. *Contrib. Mineral. Petrol.* **125**, 375-392.
Ionov D. A., Qi Y.-H., Kang J.-T., Golovin A. V., Oleinikov O. B., Zheng W., Anbar A. D., Zhang Z.-F. and Huang F. (2019) Calcium isotopic signatures of carbonatite and silicate metasomatism, melt percolation and crustal recycling in the lithospheric mantle. *Geochim. Cosmochim. Acta* **248**, 1-13.
Ionov D. A., Shirey S. B., Weis D. and Brügmann G. (2006) Os-Hf-Sr-Nd isotope and PGE systematics of spinel peridotite xenoliths from Tok, SE Siberian craton: Effects of pervasive metasomatism in shallow refractory mantle. *Earth Planet Sci Lett* **241**, 47-64.
Kang J.-T., Ionov D. A., Liu F., Zhang C.-L., Golovin A. V., Qin L.-P., Zhang Z.-F. and Huang F. (2017) Calcium isotopic fractionation in mantle peridotites by melting and metasomatism and Ca isotope composition of the Bulk Silicate Earth. *Earth Planet Sci Lett* **474**, 128-137.
Kang J.-T., Ionov D. A., Zhu H.-L., Liu F., Zhang Z.-F., Liu Z. and Huang F. (2019) Calcium isotope sources and fractionation during melt-rock interaction in the lithospheric mantle: Evidence from pyroxenites, wehrlites, and eclogites. *Chem. Geol.* **524**, 272-282.
Kang J.-T., Zhou C., Huang J.-Y., Hao Y.-T., Liu F., Zhu H.-L., Zhang Z.-F. and Huang F.

(2020) Diffusion-driven Ca-Fe isotope fractionations in the upper mantle: Implications for mantle cooling and melt infiltration. *Geochim. Cosmochim. Acta* **290**, 41-58.

Kang J.-T., Zhu H.-L., Liu Y.-F., Liu F., Wu F., Hao Y.-T., Zhi X.-C., Zhang Z.-F. and Huang F. (2016) Calcium isotopic composition of mantle xenoliths and minerals from Eastern China. *Geochim. Cosmochim. Acta* **174**, 335-344.

Katayama I., Suyama Y., Ando J.-i. and Komiya T. (2009) Mineral chemistry and P-T condition of granular and sheared peridotite xenoliths from Kimberley, South Africa: Origin of the textural variation in the cratonic mantle. *Lithos* **109**, 333-340.

Kramers J. D., Roddick J. C. M. and Dawson J. B. (1983) Trace element and isotope studies on veined, metasomatic and "MARID" xenoliths from Bultfontein, South Africa. *Earth Planet Sci Lett* **65**, 90-106.

Laurora A., Mazzucchelli M., Rivalenti G., Vannucci R., Zanetti A., Barbieri M. A. and Cingolani C. A. (2001) Metasomatism and melting in carbonated peridotite xenoliths from the mantle wedge: The Gobernador Gregores case (southern Patagonia). *J. Petrol.* **42**, 69-87.

Li C. F., Li X. H., Li Q. L., Guo J. H., Li X. H. and Yang Y. H. (2012) Rapid and precise determination of Sr and Nd isotopic ratios in geological samples from the same filament loading by thermal ionization mass spectrometry employing a single-step separation scheme. *Anal Chim Acta* **727**, 54-60.

Liu F., Li X., Wang G., Liu Y., Zhu H., Kang J., Huang F., Sun W., Xia X. and Zhang Z. (2017a) Marine carbonate component in the mantle beneath the southeastern Tibetan Plateau: evidence from magnesium and calcium isotopes. *J. Geophys. Res. Solid Earth* **122**, 9729-9744.

Liu F., Zhu H. L., Li X., Wang G. Q. and Zhang Z. F. (2017b) Calcium Isotopic Fractionation and Compositions of Geochemical Reference Materials. *Geostand Geoanal Res* **41**, 675-688.

Liu J., Carlson R. W., Rudnick R. L., Walker R. J., Gao S. and Wu F.-y. (2012) Comparative Sr–Nd–Hf–Os–Pb isotope systematics of xenolithic peridotites from Yangyuan, North China Craton: Additional evidence for a Paleoproterozoic age. *Chem Geol* **332–333**, 1-14.

Luo Y., Qin H., Wu T. and Li Z. (2020) Petrogenesis of the Granites in the Yandangshan Area, Southeastern China: Constraints from SHRIMP U-Pb Zircon Age and Trace Elements, and Sr-Nd-Hf Isotopic Data. *J. Earth Sci.* **31**, 693-708.

Ma J., Wei G., Liu Y., Ren Z., Xu Y. and Yang Y. (2013) Precise measurement of stable neodymium isotopes of geological materials by using MC-ICP-MS. *JAAS* **28**, 1926-1931.

McDonough W. F. and Sun S.-s. (1995) The composition of the Earth. *Chem Geol* **120**, 223-253.

Meng F., Xu W., Xu Q., Guo J. and Zhang Y. (2019) Decoupling of Lu-Hf and Sm-Nd Isotopic System in Deep-Seated Xenoliths from the Xuzhou-Suzhou Area, China: Differences in Element Mobility during Metamorphism. *J. Earth Sci.* **30**, 1266-1279.

Navon O. and Stolper E. (1987) Geochemical consequences of melt percolation: the upper mantle as a chromatographic column. *Journal of Geology* **95**, 285-307.

Pearson D. G., Canil D. and Shirey S. B. (2014) Mantle samples included in volcanic rocks: Xenoliths and diamonds, in: Carlson, R.W. (Ed.), Treatise on Geochemistry (Second Edition). Elsevier, Oxford, pp. 169-253.

Rivalenti G., Zanetti A., Mazzucchelli M., Vannucci R. and Cingolani C. A. (2004) Equivocal carbonatite markers in the mantle xenoliths of the Patagonia backarc: the Gobernador Gregores case (Santa Cruz Province, Argentina). *Contrib. Mineral. Petrol.* **147**, 647-670.

Rudnick R. L., McDonough W. F. and Chappell B. C. (1993) Carbonatite metasomatism in the northern Tanzanian mantle. *Earth Planet Sci Lett* **114**, 463-475.

Skulan J., DePaolo D. J. and Owens T. L. (1997) Biological control of calcium isotopic abundances in the global calcium cycle. *Geochim. Cosmochim. Acta* **61**, 2505-2510.

Stracke A. (2012) Earth's heterogeneous mantle: A product of convection-driven interaction between crust and mantle. *Chem Geol* **330–331**, 274-299.

Streckeisen A. (1976) To each plutonic rock its proper name. *Earth Sci. Rev.* **12**, 1-33.

Sun J., Zhu X. K., Belshaw N. S., Chen W., Doroshkevich A. G., Luo W. J., Song W. L., Chen B. B., Cheng Z. G., Li Z. H., Wang Y., Kynicky J. and Henderson G. M. (2021) Ca isotope systematics of carbonatites: Insights into carbonatite source and evolution. *Geochemical Perspectives Letters* **17**, 11-15.

Tanaka T., Togashi S., Kamioka H., Amakawa H., Kagami H., Hamamoto T., Yuhara M., Orihashi Y., Yoneda S., Shimizu H., Kunimaru T., Takahashi K., Yanagi T., Nakano T., Fujimaki H., Shinjo R., Asahara Y., Tanimizu M. and Dragusanu C. (2000) JNdi-1: a neodymium isotopic reference in consistency with LaJolla neodymium. *Chem Geol* **168**, 279-281.

Tang W., Hui H., Ionov D. A., Chen W., Zhang L. and Xu Y. (2020) Metasomatism-controlled hydrogen distribution in the Spitsbergen upper mantle. *Am. Mineral.* **105**, 1326-1341.

Tappe S., Romer R. L., Stracke A., Steenfelt A., Smart K. A., Muehlenbachs K. and Torsvik T. H. (2017) Sources and mobility of carbonate melts beneath cratons, with implications for deep carbon cycling, metasomatism and rift initiation. *Earth Planet Sci Lett* **466**, 152-167.

Tappe S., Stracke A., van Acken D., Strauss H. and Luguet A. (2020) Origins of kimberlites and carbonatites during continental collision – Insights beyond decoupled Nd-Hf isotopes. *Earth-Science Reviews* **208**, 103287.

Thirlwall M. F. (1991) Long-term reproducibility of multicollector Sr and Nd isotope ratio analysis. *Chem. Geol.* **94**, 85-104.

Vagnes E. and Amundsen H. E. F. (1993) Late Cenozoic uplift and volcanism on Spitsbergen: Caused by mantle convection? *Geology* **21**, 251-254.

Valdes M. C., Moreira M., Foriel J. and Moynier F. (2014) The nature of Earth's building blocks as revealed by calcium isotopes. *Earth Planet Sci Lett* **394**, 135-145.

van der Meer Q. H. A., Klaver M., Waight T. E. and Davies G. R. (2013) The provenance of sub-cratonic mantle beneath the Limpopo Mobile Belt (South Africa). *Lithos* **170–171**, 90-104.

Wang Z., Ma J., Li J., Wei G., Zeng T., Li L., Zhang L., Deng W., Xie L. and Liu Z. (2018) Fe (hydro) oxide controls Mo isotope fractionation during the weathering of granite. *Geochim. Cosmochim. Acta* **226**, 1-17.

Weis D., Kieffer B., Maerschalk C., Barling J., de Jong J., Williams G. A., Hanano D., Pretorius W., Mattielli N., Scoates J. S., Goolaerts A., Friedman R. M. and Mahoney J. B. (2006) High-precision isotopic characterization of USGS reference materials by TIMS and

MC-ICP-MS. *Geochem. Geophys. Geosyst.* **7**.

Workman R. K. and Hart S. R. (2005) Major and trace element composition of the depleted MORB mantle (DMM). *Earth Planet Sci Lett* **231**, 53-72.

Xu M., Jing Z., Bajgain S. K., Mookherjee M., Van Orman J. A., Yu T. and Wang Y. (2020) High-pressure elastic properties of dolomite melt supporting carbonate-induced melting in deep upper mantle. *Proc. Natl. Acad. Sci. USA*, 202004347.

Xu Y. (2002) Evidence for crustal components in the mantle and constraints on crustal recycling mechanisms: pyroxenite xenoliths from Hannuoba, North China. *Chem. Geol.* **182**, 301-322.

Yaxley G. M., Crawford A. J. and Green D. H. (1991) Evidence for carbonatite metasomatism in spinel peridotite xenoliths from western Victoria, Australia. *Earth Planet Sci Lett* **107**, 305-317.

Yaxley G. M., Green D. H. and Kamenetsky V. (1998) Carbonate metasomatism in the southeastern Australian lithosphere. *J. Petrol.* **39**, 1917-1931.

Zhao X., Zhang Z., Huang S., Liu Y., Li X. and Zhang H. (2017) Coupled extremely light Ca and Fe isotopes in peridotites. *Geochim. Cosmochim. Acta* **208**, 368-380.

Zhu H., Du L., Li X., Zhang Z. and Sun W. (2020) Calcium isotopic fractionation during plate subduction: Constraints from back-arc basin basalts. *Geochim. Cosmochim. Acta* **270**, 379-393.

Zhu H., Liu F., Li X., An Y., Wang G. and Zhang Z. (2018a) A “peak cut” procedure of column separation for calcium isotope measurement using the double spike technique and thermal ionization mass spectrometry (TIMS). *J. Anal. At. Spectrom.* **33**, 547-554.

Zhu H., Liu F., Li X., Wang G., Zhang Z. and Sun W. (2018b) Calcium isotopic compositions of normal Mid-Ocean Ridge basalts from the southern Juan de Fuca Ridge. *J. Geophys. Res. Solid Earth* **123**, 1303-1313.

Zhu H. L., Zhang Z. F., Wang G. Q., Liu Y. F., Liu F., Li X. and Sun W. D. (2016) Calcium Isotopic Fractionation during Ion-Exchange Column Chemistry and Thermal Ionisation Mass Spectrometry (TIMS) Determination. *Geostand. Geoanal. Res.* **40**, 185-194.

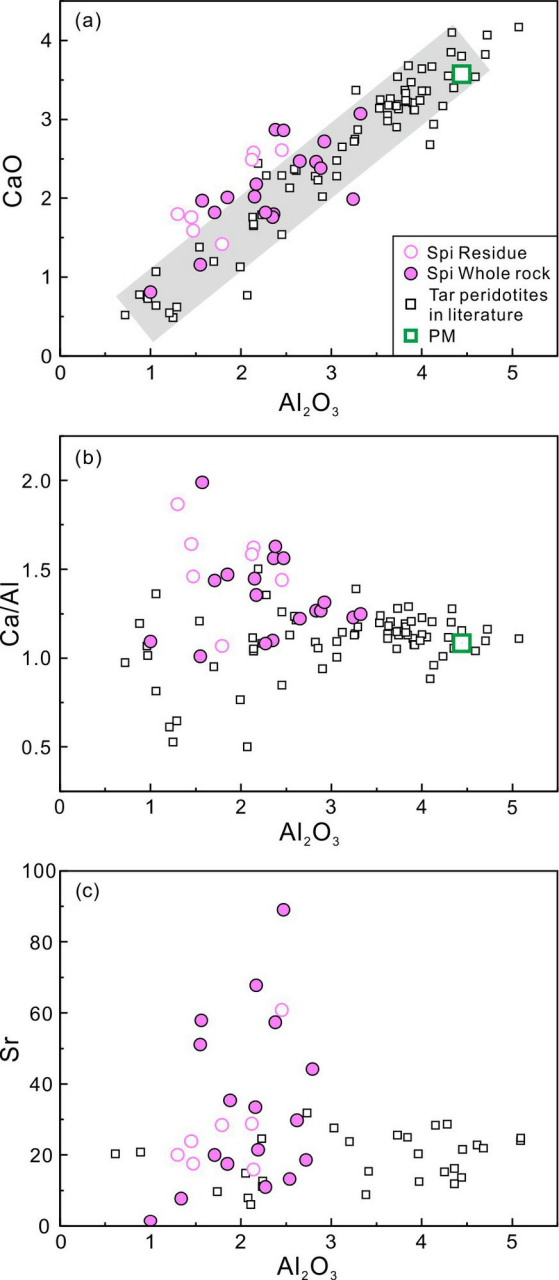
(a)
CaO
Al2O3
Spi Residue
Spi Whole rock
Tar peridotites in literature
PM
(b)
Ca/Al
Al2O3
(c)
Sr
Al2O3

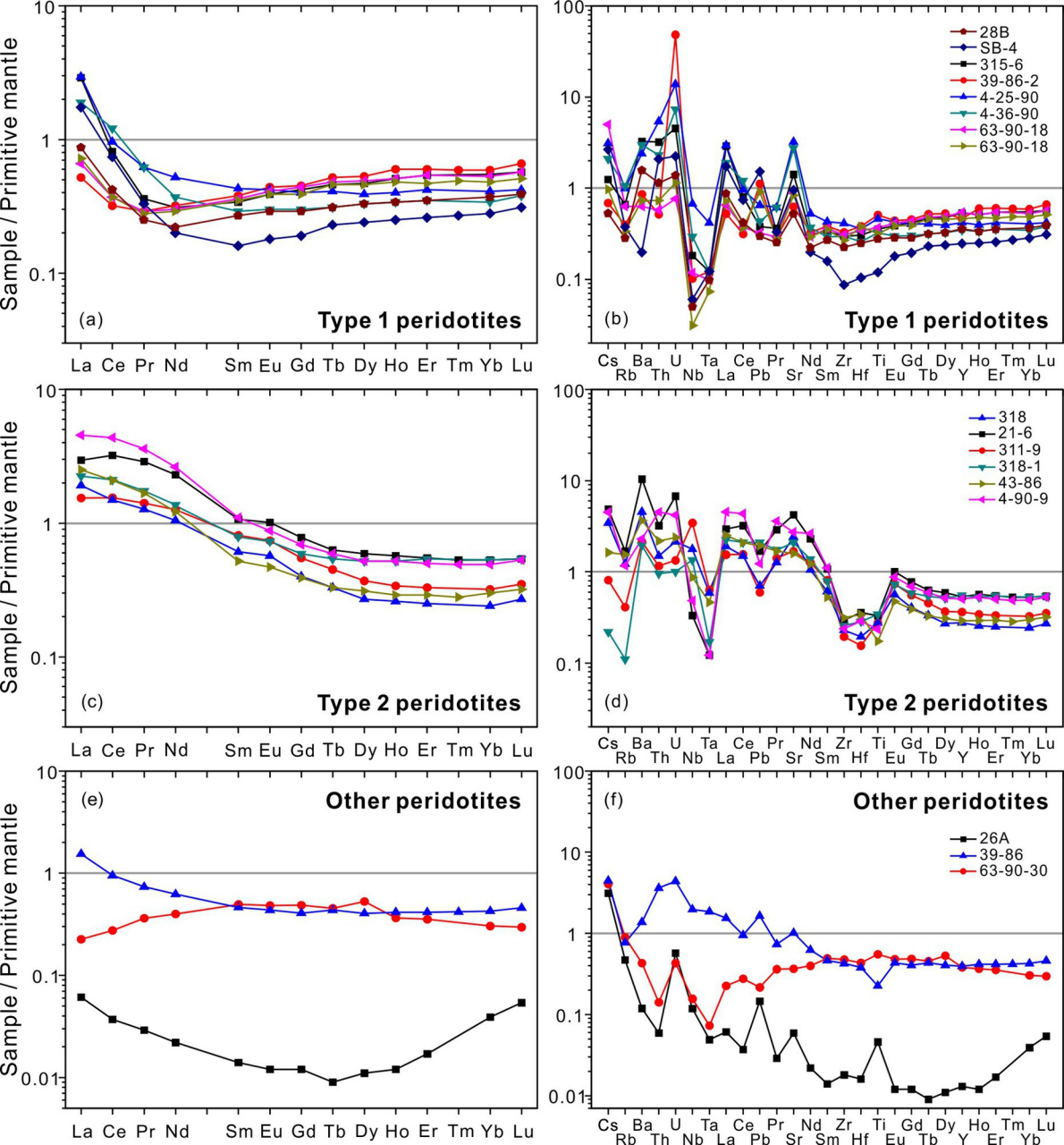
Sample / Primitive mantle
(a)
Type 1 peridotites
La Ce Pr Nd Sm Eu Gd Tb Dy Ho Er Tm Yb Lu
(b)
Type 1 peridotites
28B
SB-4
315-6
39-86-2
4-25-90
4-36-90
63-90-18
63-90-18
Cs Ba U Ta Ce Pr Nd Zr Ti Gd Dy Ho Tm Lu
Rb Th Nb La Pb Sr Sm Hf Eu Tb Y Er Yb
(c)
Type 2 peridotites
(d)
Type 2 peridotites
318
21-6
311-9
318-1
43-86
4-90-9
(e)
Other peridotites
(f)
Other peridotites
26A
39-86
63-90-30

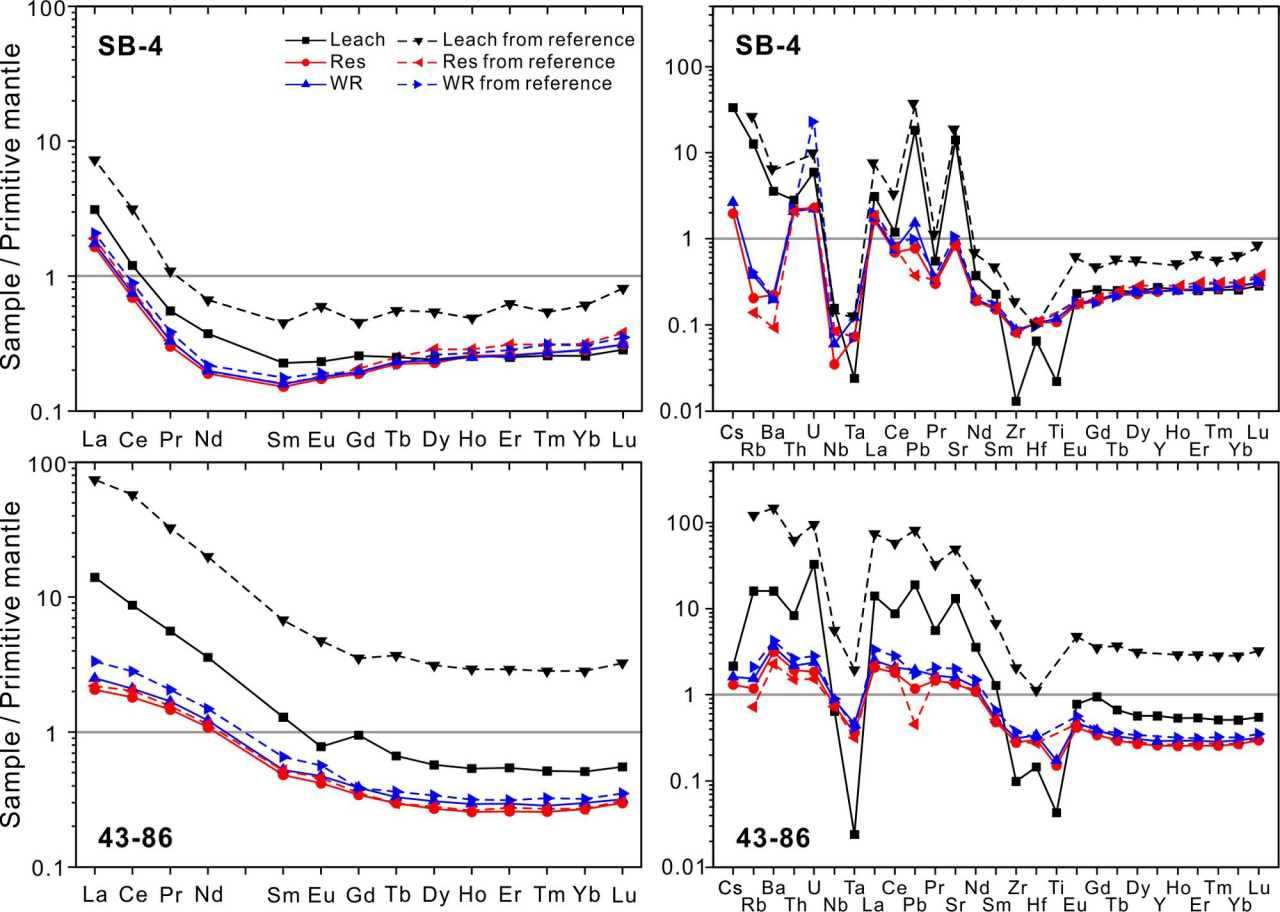
SB-4
Leach
Res
WR
Leach from reference
Res from reference
WR from reference
Sample / Primitive mantle
100
10
1
0.1
0.01
La Ce Pr Nd Sm Eu Gd Tb Dy Ho Er Tm Yb Lu
Cs Rb Ba Th U Nb Ta La Ce Pb Pr Sr Nd Sm Zr Hf Ti Eu Gd Tb Dy Y Ho Er Tm Yb Lu
43-86

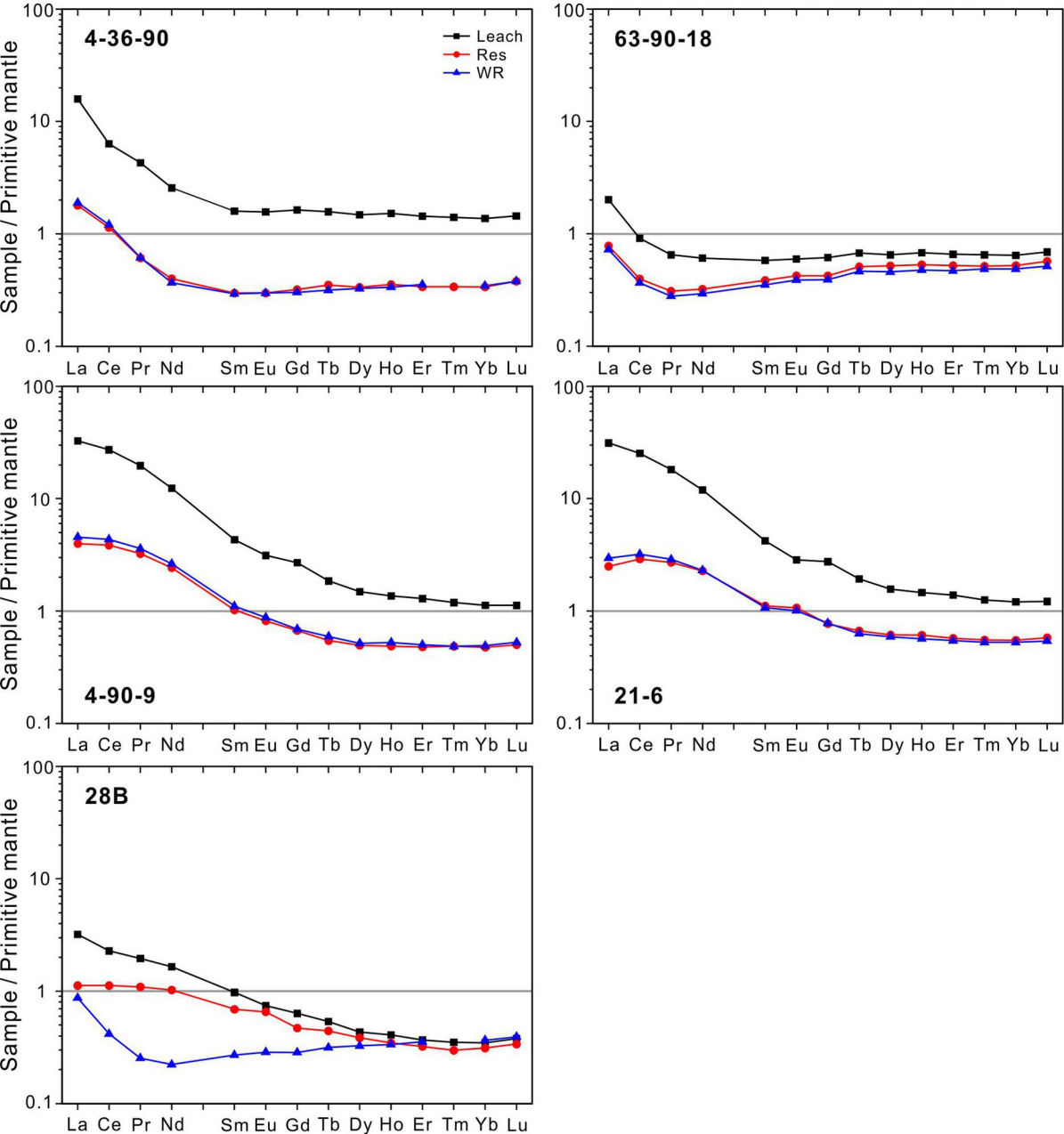
4-36-90
Leach
Res
WR
63-90-18
4-90-9
21-6
28B
Sample / Primitive mantle
100
10
1
0.1
La Ce Pr Nd Sm Eu Gd Tb Dy Ho Er Tm Yb Lu

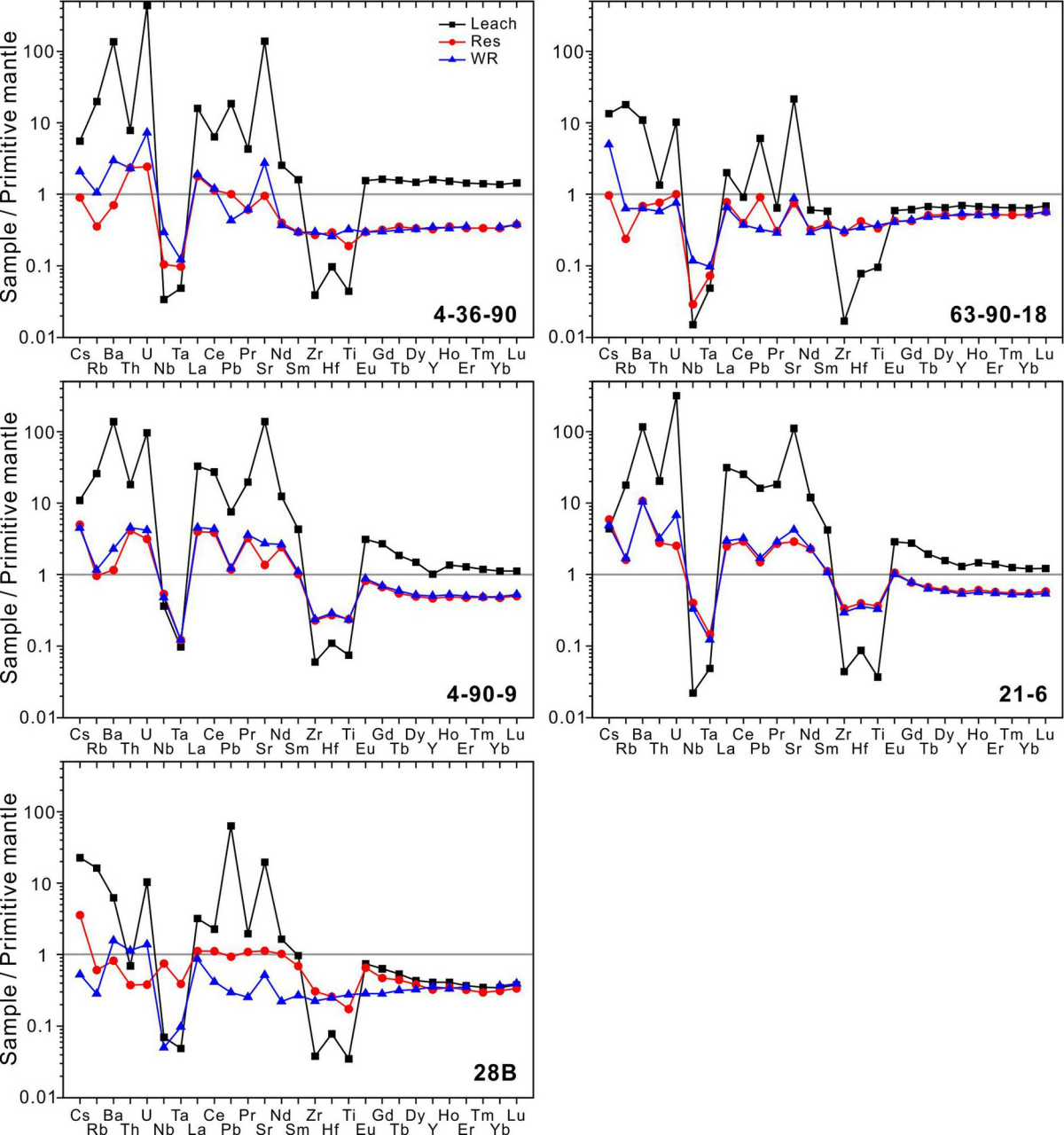
Leach
Res
WR
Sample / Primitive mantle
100
10
1
0.1
0.01
4-36-90
63-90-18
4-90-9
21-6
28B
Cs Ba U Ta Ce Pr Nd Zr Ti Gd Dy Ho Tm Lu
Rb Th Nb La Pb Sr Sm Hf Eu Tb Y Er Yb

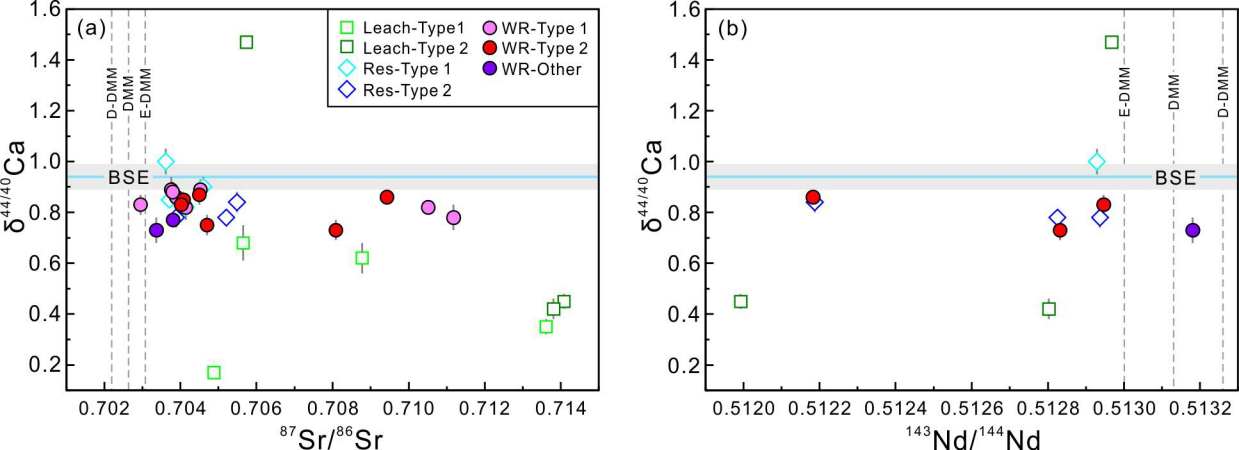
(a)
Leach-Type1
Leach-Type 2
Res-Type 1
Res-Type 2
WR-Type 1
WR-Type 2
WR-Other
D-DMM
DMM
E-DMM
BSE
δ44/40Ca
87Sr/86Sr
(b)
E-DMM
DMM
D-DMM
BSE
δ44/40Ca
143Nd/144Nd

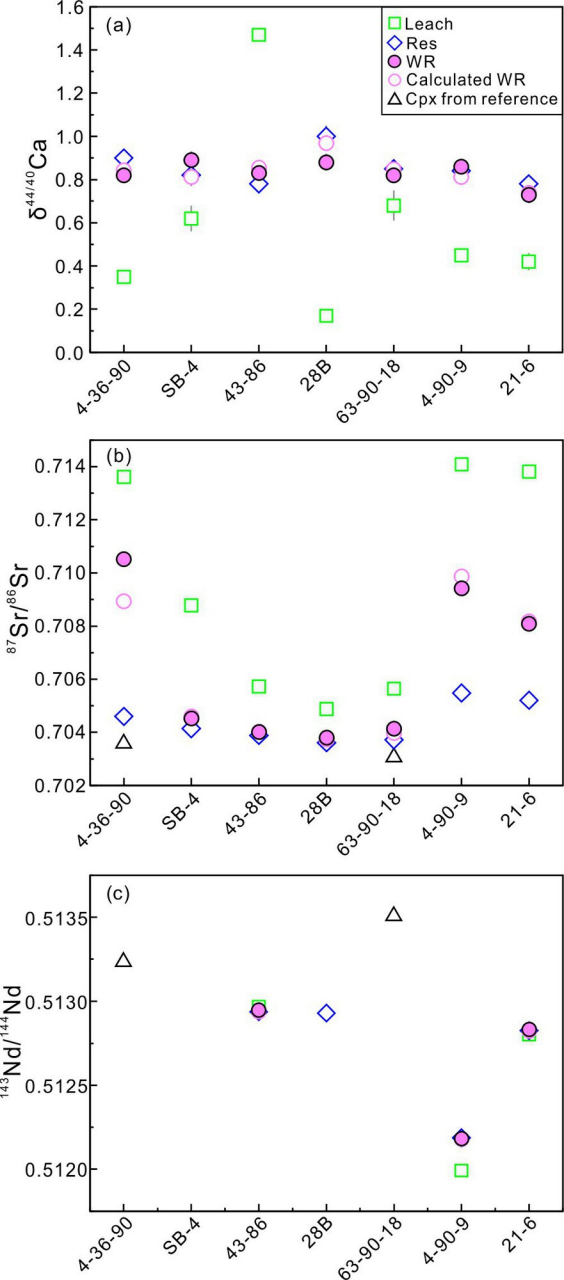
(a)
Leach
Res
WR
Calculated WR
Cpx from reference
δ44/40Ca
1.6
1.4
1.2
1.0
0.8
0.6
0.4
0.2
0.0
4-36-90
SB-4
43-86
28B
63-90-18
4-90-9
21-6
(b)
87Sr/86Sr
0.714
0.712
0.710
0.708
0.706
0.704
0.702
4-36-90
SB-4
43-86
28B
63-90-18
4-90-9
21-6
(c)
143Nd/144Nd
0.5135
0.5130
0.5125
0.5120
4-36-90
SB-4
43-86
28B
63-90-18
4-90-9
21-6

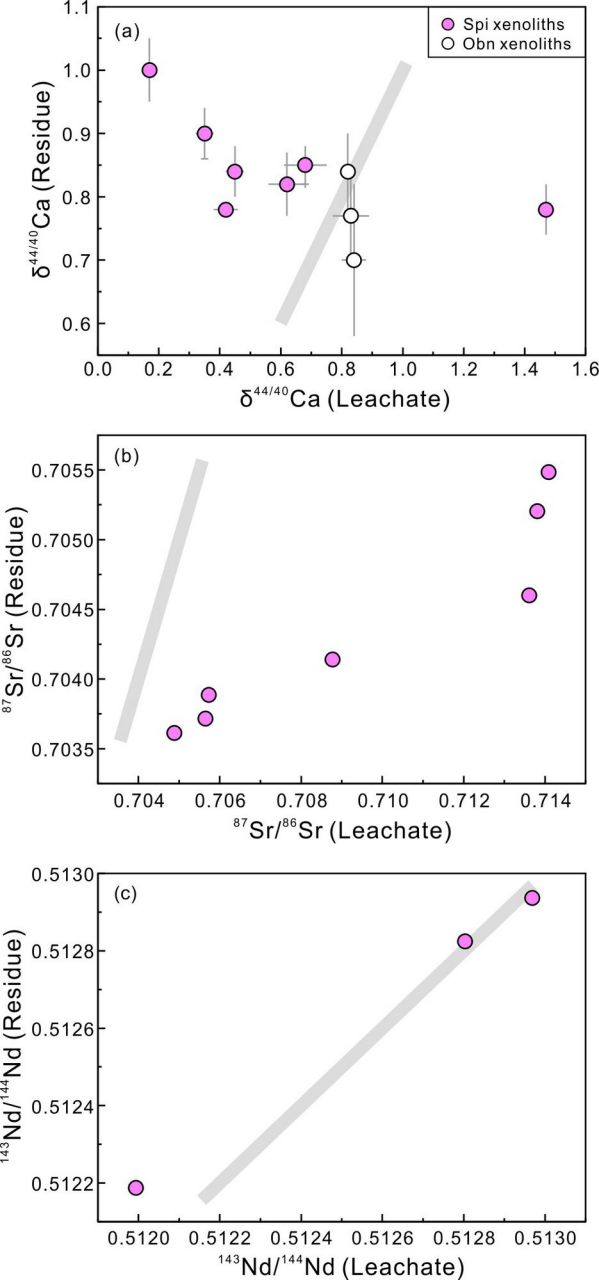
(a)
Spi xenoliths
Obn xenoliths
δ44/40Ca (Residue)
δ44/40Ca (Leachate)
1.1
1.0
0.9
0.8
0.7
0.6
0.0
0.2
0.4
0.6
0.8
1.0
1.2
1.4
1.6
(b)
87Sr/86Sr (Residue)
87Sr/86Sr (Leachate)
0.7055
0.7050
0.7045
0.7040
0.7035
0.704
0.706
0.708
0.710
0.712
0.714
(c)
143Nd/144Nd (Residue)
143Nd/144Nd (Leachate)
0.5130
0.5128
0.5126
0.5124
0.5122
0.5120
0.5122
0.5124
0.5126
0.5128
0.5130

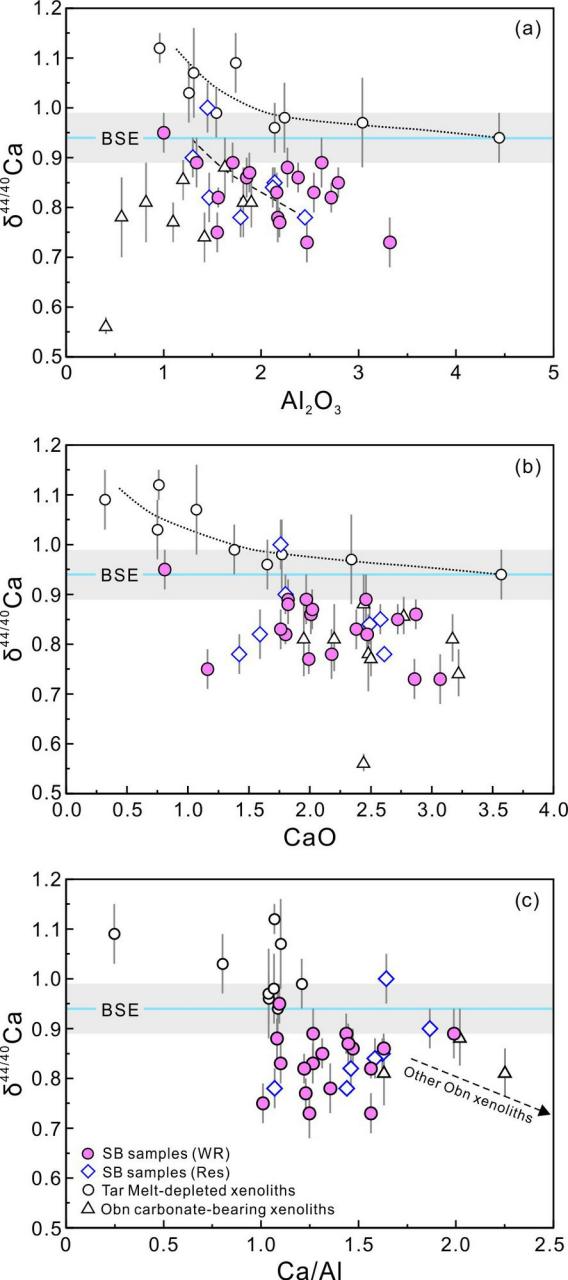
(a)
BSE
δ44/40Ca
Al2O3
(b)
BSE
δ44/40Ca
CaO
(c)
BSE
δ44/40Ca
Ca/Al
Other Obn xenoliths
SB samples (WR)
SB samples (Res)
Tar Melt-depleted xenoliths
Obn carbonate-bearing xenoliths

Table 1. Sample list and information summary for the Spitsbergen xenoliths.

Sample	Location	Rock type[a]	Leaching	Data source[b]														
				Major elements			Trace elements			Sr isotopes			Nd isotopes			Ca isotopes		
				WR	Res	Leach	WR	Res	Leach	WR	Res	Leach	WR	Res	Leach	WR	Res	Leach
4-36-90*	Halvdan	Spl Lh	×	×, (3)	×	×	(2)	×	×	×	×	×				×	×	×
4-90-9*	Halvdan	Spl Lh	×	×	×	×	×	×	×	×	×	×	×	×	×	×	×	×
21-6*	Halvdan	Spl Lh	×	×	×	×	×	×	×	×	×	×	×	×	×	×	×	×
43-86*	Sverre	Spl Lh	×	×, (3)	×	×	×, (1)	×, (1)	×, (1)	×	×	×	×	×	×	×	×	×
28B	Sverre	Spl Lh	×	(3)	×	×	(2)	×	×	×	×	×		×		×	×	×
63-90-18	Sverre	Spl Lh	×	×, (3)	×	×	(2)	×	×	×	×	×				×	×	×
SB-4	Halvdan	Spl Lh	×	×	×	×	×, (1)	×, (1)	×, (1)	×	×	×				×	×	×
315-6	Halvdan	Spl Lh		×, (2)			(2)			×						×		
39-86-2	Sverre	Spl Lh		×, (2)			(2)			×						×		
4-25-90	Halvdan	Spl Lh		(2)			(2)			×						×		
63-90-18-1	Sverre	Spl Lh		×			×			×						×		
311-9	Halvdan	Spl Lh		×, (2)			(2)			×						×		
318	Halvdan	Hz		(2)			(2)			×						×		
318-1	Halvdan	Spl Lh		×, (2)			(2)			×						×		
26A	Sverre	Hz		(2)			(2)									×		
63-90-30	Sverre	Spl Lh		×, (2)			(2)									×		
39-86	Sverre	Spl Lh		×, (3)			×			×						×		
4A-90-1-Cpx	Sigurd	Amph Wh								(4)			(4)			×		
4A-90-1-Amph	Sigurd	Amph Wh								(4)			(4)			×		

[a] Abbreviations: Spl Lh, spinel lherzolite; Hz, harzburgite; Wh, wehrlite; Cpx, clinopyroxene; Amph, amphibole; WR, whole-rock; Res, residues; Leach, leachates. *Samples that contain the largest and most abundant carbonate aggregates.

[b] Data sources: ×, this study; (1) Ionov et al. (1993); (2) Ionov et al. (2002a); (3) Ionov et al. (1996); (4) Ionov et al. (2002b).

Table 2. Ca-Sr-Nd isotopic compositions of reference samples.

		$\delta^{44/40}Ca$	2SD[a]	n[b]	$^{87}Sr/^{86}Sr$	2SD	n	$^{143}Nd/^{144}Nd$	2SD	n
NIST SRM 915a	This study	-0.02	0.12	21						
	Huang et al. (2010)	0.04	0.13	45						
	Valdes et al. (2014)	0.00	0.17	74						
IAPSO seawater	This study	1.82	0.10	10						
	Farkaš et al. (2007)	1.86	0.20	5						
	He et al. (2017)	1.89	0.18	147						
DTS-1	This study	1.61	0.09	3						
	Huang et al. (2010)	1.59	0.16	3						
	Feng et al. (2017)	1.51	0.13	7						
DTS-2	This study	1.10	0.11	3						
	Feng et al. (2017)	1.20	0.11	9						
PCC-1	This study	1.10	0.08	3						
	Amini et al. (2009)	1.15	0.09	13						
BHVO-2	This study	0.84	0.09	5	0.703503		1			
	Valdes et al. (2014)	0.87	0.16	10						
	He et al. (2017)	0.79	0.09	7						
	Weis et al. (2006)				0.703487	0.000019	12			
NBS-987	This study				0.710254	0.000014	12			
	Thirlwall (1991)				0.710248	0.000011	427			
	Charlier et al. (2006)				0.710255	0.000018	222			
JNdi-1	This study							0.512111	0.000013	14
	Tanaka et al. (2000)							0.512115	0.000007	
	Li et al. (2012)							0.512113	0.000012	5
W-2	This study							0.512512		1
	Li et al. (2012)							0.512518	0.000006	2

[a] 2SD: two standard deviations.

[b] n: number of replicate Ca-Sr-Nd isotope analyses.

Table 3. Ca-Sr-Nd isotopic compositions of leachates, residues, whole-rocks (WR) and calculated WR for carbonate-bearing xenoliths.

Sample		Mass fraction	Ca fraction	$\delta^{44/40}$Ca	2SD	2SE[a]	n	Sr fraction	^{87}Sr/^{86}Sr[c]	Nd fraction	^{143}Nd/^{144}Nd[c]
4-36-90	Leachate	0.006	0.10	0.35	0.05	0.03	3	0.48	0.713612	0.04	
	Residue	0.994	0.90	0.90	0.07	0.04	3	0.52	0.704601	0.96	
	Whole Rock	1.000	1.00	0.82	0.03	0.02	3	1.00	0.710515	1.00	
	Calculated WR			0.84					0.708932		
4-90-9	Leachate	0.010	0.08	0.45	0.05	0.03	3	0.51	0.714085	0.05	0.511993
	Residue	0.990	0.92	0.84	0.08	0.04	3	0.49	0.705484	0.95	0.512187
	Whole Rock	1.000	1.00	0.86	0.06	0.03	3	1.00	0.709426	1.00	0.512183
	Calculated WR			0.81					0.709869		0.512178
21-6	Leachate	0.014	0.12	0.42	0.07	0.04	3	0.35	0.713810	0.07	0.512803
	Residue	0.986	0.88	0.78	0.02	0.01	3	0.65	0.705203	0.93	0.512825
	Whole Rock	1.000	1.00	0.73	0.06	0.04	3	1.00	0.708086	1.00	0.512832
	Calculated WR			0.74					0.708175		0.512823
43-86	Leachate	0.009	0.11	1.47	0.03	0.02	3	0.08	0.705733	0.03	0.512968
	Leachate-R[b]			1.46	0.08	0.05	3				
	Residue	0.991	0.89	0.78	0.09	0.04	4	0.92	0.703886	0.97	0.512937
	Whole Rock	1.000	1.00	0.85	0.13	0.07	3	1.00	0.704016	1.00	0.512938
	Whole Rock-R[b]			0.82			2		0.704023		0.512956
	Calculated WR			0.86					0.704029		0.512938
SB-4	Leachate	0.007	0.03	0.62	0.10	0.06	3	0.10	0.708775	0.01	
	Residue	0.993	0.97	0.82	0.09	0.05	3	0.90	0.704142	0.99	
	Whole Rock	1.000	1.00	0.89	0.06	0.04	3	1.00	0.704527	1.00	
	Calculated WR			0.81					0.704604		
28B	Leachate	0.006	0.04	0.17	0.02	0.01	3	0.10	0.704880	0.01	
	Residue	0.994	0.96	1.00	0.09	0.05	3	0.90	0.703615	0.99	0.512929
	Whole Rock	1.000	1.00	0.88	0.06	0.04	3	1.00	0.703799	1.00	
	Calculated WR			0.97					0.703742		
63-90-18	Leachate	0.006	0.03	0.68	0.11	0.07	3	0.14	0.705647	0.01	
	Residue	0.994	0.97	0.85	0.05	0.03	3	0.86	0.703716	0.99	
	Whole Rock	1.000	1.00	0.83	0.05	0.03	3	1.00	0.704138	1.00	
	Whole Rock-R[b]			0.80			1		0.704133		
	Calculated WR			0.85					0.703980		

[a] 2SE: two standard deviations of the mean. 2SE = 2SD/sqrt(n).

[b] R: repeated dissolution and analysis for two whole rocks and a repeated analysis for one leachate.

[c] Sr-Nd isotopes of leachate, residue and whole rock of carbonate-bearing xenoliths are measured once。

Table 4. Ca-Sr-Nd isotopic compositions of non-leached whole-rock Spitsbergen xenoliths and minerals.

Sample		$\delta^{44/40}$Ca	2SD	2SE	n	^{87}Sr/^{86}Sr[a]	^{143}Nd/^{144}Nd
315-6	Whole rock	0.89	0.09	0.05	3	0.703760	
39-86-2	Whole rock	0.83	0.07	0.04	3	0.702950	
4-25-90	Whole rock	0.78	0.12	0.05	7	0.711183	
63-90-18-1	Whole rock	0.86	0.08	0.04	3	0.703893	
311-9	Whole rock	0.87	0.06	0.04	3	0.704491	
318	Whole rock	0.75	0.06	0.04	3	0.704696	
318-1	Whole rock	0.85	0.05	0.03	3	0.704079	
26A	Whole rock	0.95	0.07	0.04	3		
63-90-30	Whole rock	0.89	0.08	0.05	3		
39-86	Whole rock	0.77	0.06	0.03	3	0.703805	
4A-90-1-Cpx[b]	Cpx mineral	1.05	0.09	0.05	3	0.703950[c]	0.512904[c]
4A-90-1-Amph[b]	Amph mineral	0.97	0.09	0.05	3	0.704000[c]	0.512894[c]

[a] Single Sr isotope analyses for non-leached whole-rock xenoliths.

[b] Mineral abbreviations: cpx, clinopyroxene; amph, amphibole.

[c] Sr and Nd isotopic compositions of cpx and amph in sample 4A-90-1 are from Ionov et al. (2002b).